LUMIN

Final Report

on

Contract NAS8-32147

DUAL HOLOGRAM DESIGN STUDY

by

Hua-Kuang Liu

Prepared for

National Aeronautics and Space Administration
George C. Marshall Space Flight Center
Marshall Space Flight Center, Alabama 35812

Feburary, 1978

LUMIN Report No. 129-78

(NASA-CR-150596) DUAL HOLOGRAM DESIGN STUDY Final Report (Lumin, Inc., Tuscaloosa, Ala.) 47 p HC A03/MF A01 CSCL 14E
N78-19470
Unclas
G3/35 07333

Lumin, Inc.
P.O. BOX 5620 TUSCALOOSA, ALABAMA 35401

A PHASE-MODULATED TRIPLE-EXPOSURE HOLOGRAPHIC INTERFEROMETRIC TECHNIQUE FOR HOLOGRAPHIC NON-DESTRUCTIVE TESTING

Table of Contents

A PHASE-MODULATED TRIPLE-EXPOSURE HOLOGRAPHIC INTERFEROMETRIC TECHNIQUE FOR HOLOGRAPHIC NON-DESTRUCTIVE TESTING

Abstract

A phase-modulated triple-exposure technique is incorporated into the holographic non-destructive test (HNDT) system currently existing at NASA MSFC. The technique is able to achieve a goal of simultaneously identifying the zero-order fringe and determining the direction of motion (or displacement). Basically, the technique involves the addition of one more exposure, during the loading of the tested object, to the conventional double-exposure hologram. A phase shifter is added to either the object beam or the reference beam during the second and the third exposure.

Theoretical analysis with the assistance of computer simulation has illustrated the feasibility of implementing the phase-modulation and triple-exposure in the HNDT systems. Main advantages of the technique are the enhancement of accuracy in data interpretation and a better determination of the nature of the flaws in the tested object.

Furthermore, the concept of dual hologram fringe subtraction is also discussed. The unrealizability of this idea to the HNDT system has been demonstrated by results from computer simulation of the subtraction of fringe patterns of Fraunhofer diffraction through a single slit and the Airy rings.

A PHASE-MODULATED TRIPLE-EXPOSURE HOLOGRAPHIC INTERFEROMETRIC TECHNIQUE FOR HOLOGRAPHIC NON-DESTRUCTIVE TESTING

I. Introduction

In holographic non-destructive test (HNDT) applications, it is the inherent nature of the holographic interference patterns such that a tedius process is usually required to perform data analysis and interpretation. In addition to the complexity of the interference fringe patterns which may be given rise by the complexity of the test object and the nature of the defects, two other problems are often encountered. First is the identification of the no-motion fringe; second, the detection of the direction of motion. The fringes due to no-motion may be considered as a kind of noise that tends to blur the signal which leads to the detection of the defects in the test object, therefore, the elimination of these fringes is highly desirable. Direction of motion of the object surface is important to the determination of the nature of the flaw that caused it.

In order to achieve the purpose of isolating the fringes related to the flaws, an idea was first proposed to subtract one interference fringe from another. Through the subtraction, it was hoped that the residual fringe fragments, which constitute the difference between any two given fringe patterns, will give a simple and clear representation of the flawed regions. Any no-motion fringes will be eliminated automatically through the process since they are resulted from a common origin. Although this seemed to be an excellent idea, after careful studies, it was found that the idea cannot be realized mainly due to two factors: (1) The difficulty in the subtraction of the fringes;

(2) The impossibility of the interpretation of the results quantitatively even the subtraction is assumed to have been carried out perfectly. The difficulty in the subtraction of the fringes will be demonstrated by the technique of computer simulation as described later in the report.

Instead of the original idea of fringe subtraction, we have found that a phase-modulated triple-exposure holographic interferometric technique can be used to solve the problems of no-motion fringe identification and the detection of the direction of motion simultaneously. Section II will be a theoretical discussion of the fringe subtraction and some computer simulated results. The phase-modulated triple-exposure holographic technique will be provided in Section III. Finally, the incorporation of the technique in the HNDT system will be shown in the discussion part of Section IV.

II. Fringe Subtraction

In this section, we shall discuss the concept of fringe subtraction and show why it will not be feasible for HNDT applications.

The basic idea of fringe subtraction is to subtract one interferometric fringe pattern from another. As an example, one may consider two images, one a reference set of interferometric fringes, and the other a test set of interferometric fringes. Both of these sets of fringes are obtained by using the same object. One may assume that the first set of fringes is obtained when the object is in perfect condition and is considered as the reference set. The second set is obtained after the object has been used or its composition has been modified or degraded. If the first set of the fringes may be subtracted from the second set of fringes under ideal conditions a residual set of fringes is obtained. It is hoped that the residual set of fringes resulted from the subtraction can be used to indicate the change of composition of the object. Unfortunately, it was concluded after careful studies that this idea is not practical with regard to its potential applications to a HNDT system. We shall present our evidence as follows.

First we shall investigate three fundamental fringe patterns and discuss the subtraction of fringes based on these patterns.

(1) Fresnel zone plate

Fresnel zone plates are patterns of concentric circles, as shown in Figure 1(a), in which all black and white annuli are of equal area. It was found that when two identical zone-plate patterns that are not in concentric alignment are superimposed, fringes would appear as shown in Figure 1(b). These fringes are normal to the line of relative displacement. As it was derived in Reference 1, the number of fringes per milimeter (mm) is directly proportional to the displacement:

$$d = R^2 n \tag{1}$$

where d is the relative displacement between the two centers, mm; R is the radius of the central circle in the zone plate, mm; and n is the number of fringes per mm.

The fact that moiré fringes occur even in the case of a simple zone plate subtraction under the condition of misalignment indicated that critical and exact fringe alignment is required in our fringe subtraction subsystem.

However, zone-plate patterns obviously do not represent typical holographic interferometric fringes simply because the zone plate patterns consist

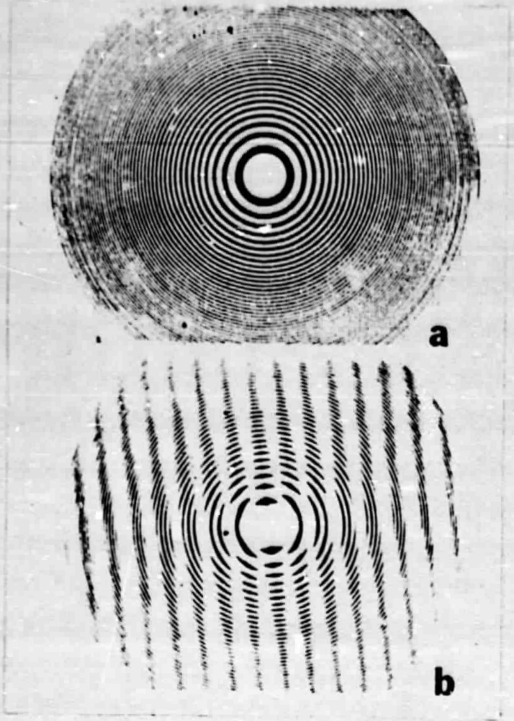

Figure 1. (a) A Fresnel zone plate pattern. (b) Supperposition of two non-concentric zone plate patterns.

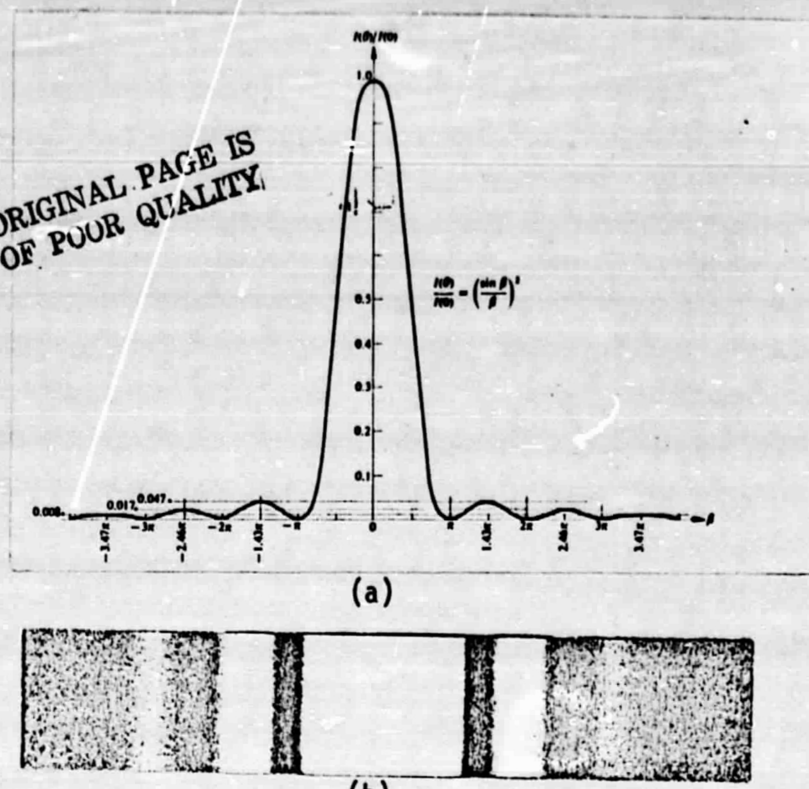

Figure 2. (a) The Fraunhofer diffraction pattern of a single slit. (b) Its experimental verification.

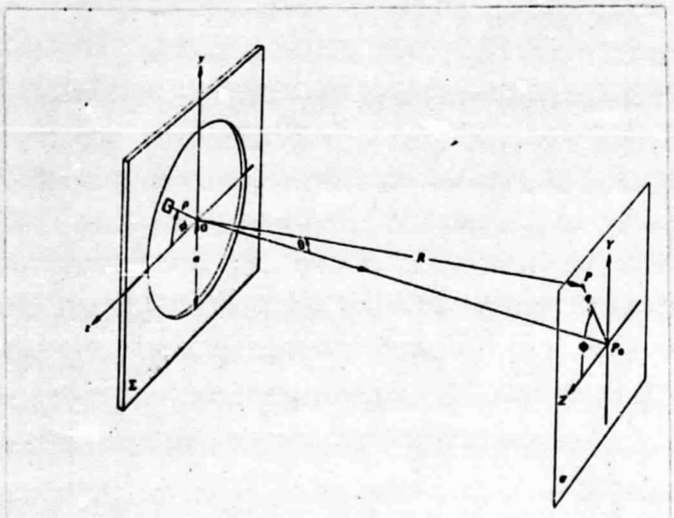

Figure 3. Circular aperture geometry.

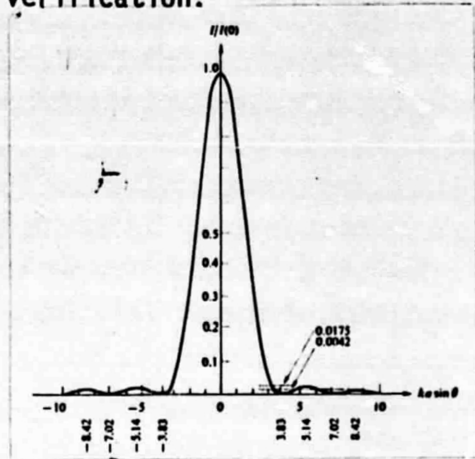

Figure 4. Normalized airy ring diffraction intensity pattern.

Figure 5. Airy rings with aperture diameter equals to (a) 0.5 mm; (b) 1.5 mm

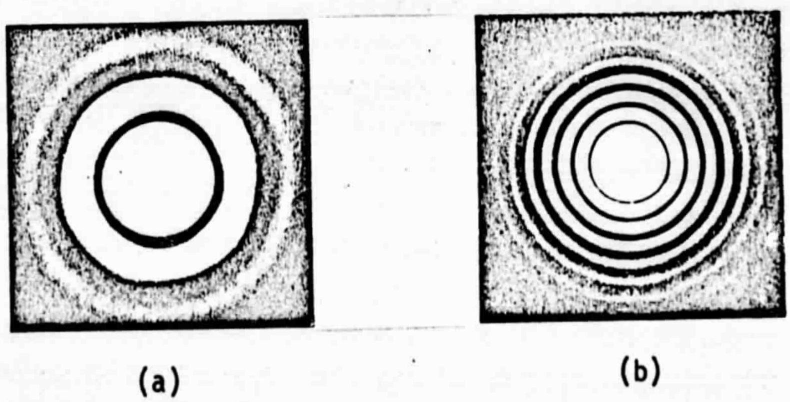

of only black (opaque) or white (transparent) rings without possessing any gray tones. Hence a second case is considered below.

(2) Fraunhofer diffraction patterns of a single slit[2].

The Fraunhofer diffraction pattern (of Eq. (2) below) of a single slit is shown in Figure 2(a) with experimental verification shown in Figure 2(b). The normalized intensity of the pattern may be written as

$$\frac{I(\theta)}{I(0)} = \left(\frac{\sin\beta}{\beta} \right)^2 \tag{2}$$

where $\beta = (Kb/2)\sin\theta$

b = width of the slit

$k = 2\pi/\lambda$

λ = wavelength of the illumination

θ = angle measured from the center of the slit to the fringe location.

The subtraction of the fringes can be analytically represented by

$$\left(a \frac{\sin\beta}{\beta} \right)^2 - \left(b \frac{\sin(\beta + \Delta\beta)}{\beta + \Delta\beta} \right)^2 \tag{3}$$

where a and b are adjustable constants representing the intensity scaling factor and $\Delta\beta$ denotes a misalignment factor.

In order to see the influence of the parameters a, b, and $\Delta\beta$ on the fringe subtraction, a computer simulation program of the problem is being implemented.

Although the diffraction pattern of a thin slit bears more resemblence to that of the holographic interferometry than the pattern of the zone plate, it is not two-dimensional. For this reason, we shall describe a third case as follows.

(3) The Airy pattern[2]

The normalized intensity distribution of the Airy pattern can be written as

$$\frac{I(\theta)}{I(0)} = \left[\frac{2J_1(k\, a \sin\theta)}{k\, a \sin\theta} \right]^2 \tag{4}$$

where J_1 is the zero order Bessel function of the first kind; and

$k = 2\pi/\lambda$

λ = wavelength of the illumination

a = radius of the circular aperture

$\theta = q/R$; q and R are shown in Figure 3.

Equation (4) is plotted and shown in Figure 4.

Photographs of the Airy rings of different apertures are shown in Figure 5.

It would also be interesting to study the difference, S, of the intensity of two fringe patterns under the influence of c, d, and $\Delta\theta$:

$$S = c\,\frac{I(\theta)}{I(0)} - d\,\frac{I(\theta + \Delta\theta)}{I(0)}\ , \tag{5}$$

where c, d are the intensity scaling parameters and $\Delta\theta$ is a factor reflecting misalignment.

Four computer programs have been written for the fringe patterns of the Fraunhofer diffraction of single slit (corresponding to Equations (2) and (3)) and the Airy fringe pattern (corresponding to Equations (4) and (5)). The computer program for Equation (2) ($\sin^2 x/x^2$) is listed as program 1; Equation (3) is listed as program 2; Equation (4) as program 3; and Equation (5) as program 4. These computer programs are listed in Appendix A.

The function $\sin^2 x/x^2$ versus x is plotted in Figure 5; due to the even symmetry of the function, it is only necessary to plot the function for negative x. The vertical coordinate of each asterisk indicates the normalized intensity of the fringes of the Fraunhofer diffraction. The function of fringe subtraction,

$$(\sin x/x)^2 - (A\ \sin(x+d)/(x+d))^2$$

versus x for positive x are plotted, with various parameters in Figures 6

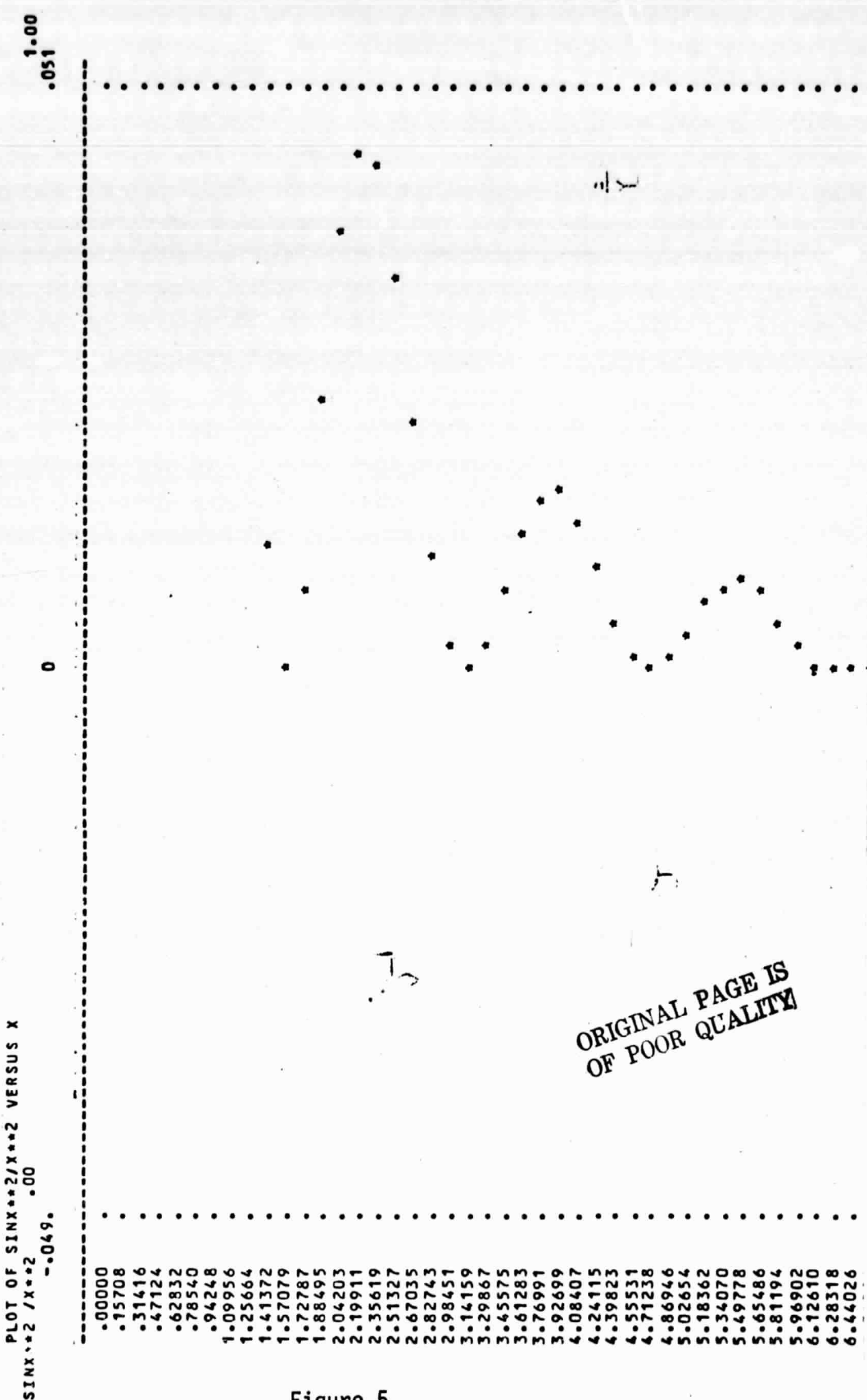
PLOT OF SINX**2/X**2 VERSUS X
SINX**2 /X**2
-.049
.00
0
.051
1.00
ORIGINAL PAGE IS
OF POOR QUALITY

Figure 5

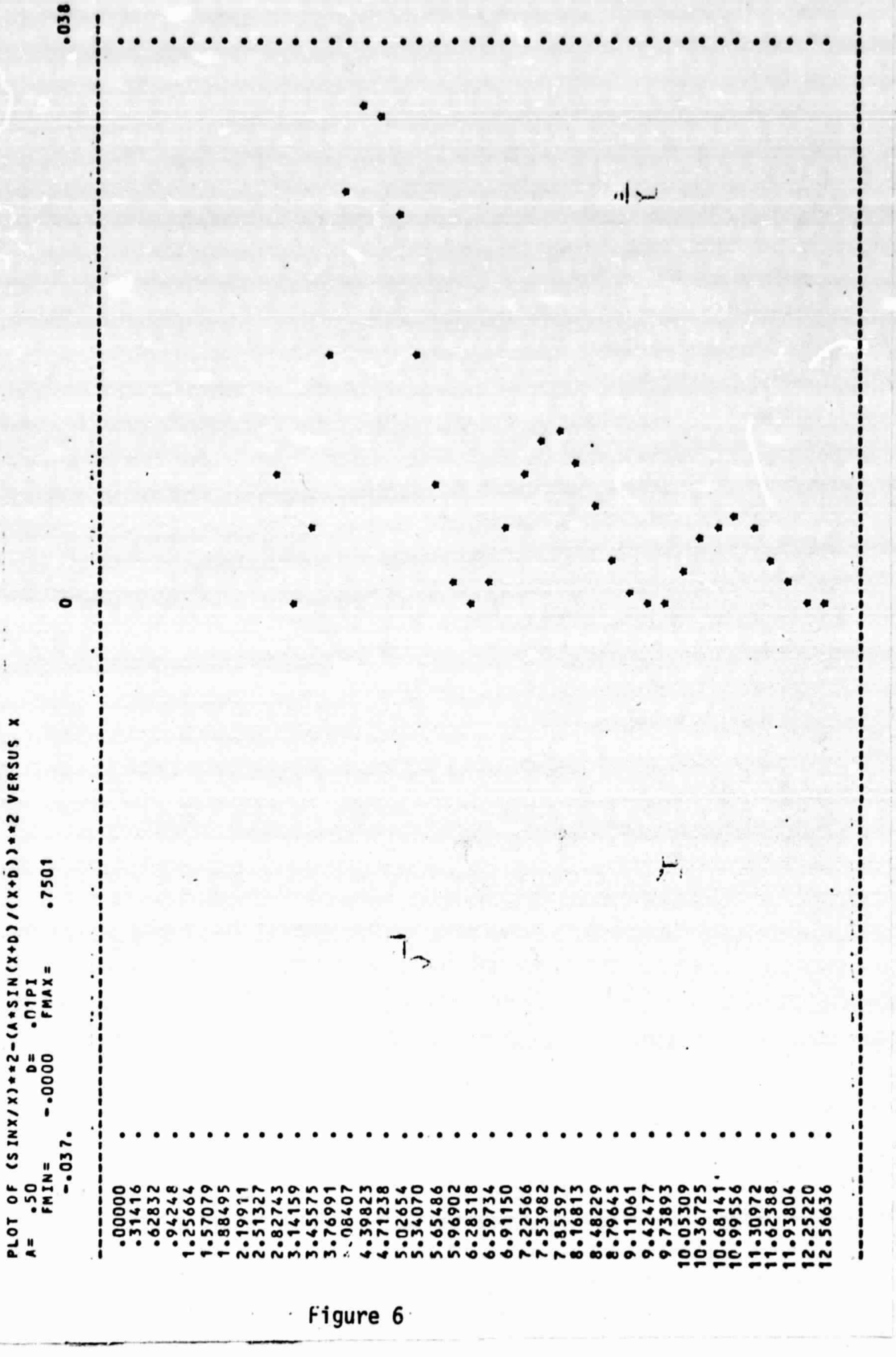
PLOT OF (SINX/X)**2-(A*SIN(X+D)/(X+D))**2 VERSUS X
A= .50 D= .01PI
FMIN= -.0000 FMAX= .7501
-.037.
0
.038
.00000
.31416
.62832
.94248
1.25664
1.57079
1.88495
2.19911
2.51327
2.82743
3.14159
3.45575
3.76991
.08407
4.39823
4.71238
5.02654
5.34070
5.65486
5.96902
6.28318
6.59734
6.91150
7.22566
7.53982
7.85397
8.16813
8.48229
8.79645
9.11061
9.42477
9.73893
10.05309
10.36725
10.68141
10.99556
11.30972
11.62388
11.93804
12.25220
12.56636

Figure 6

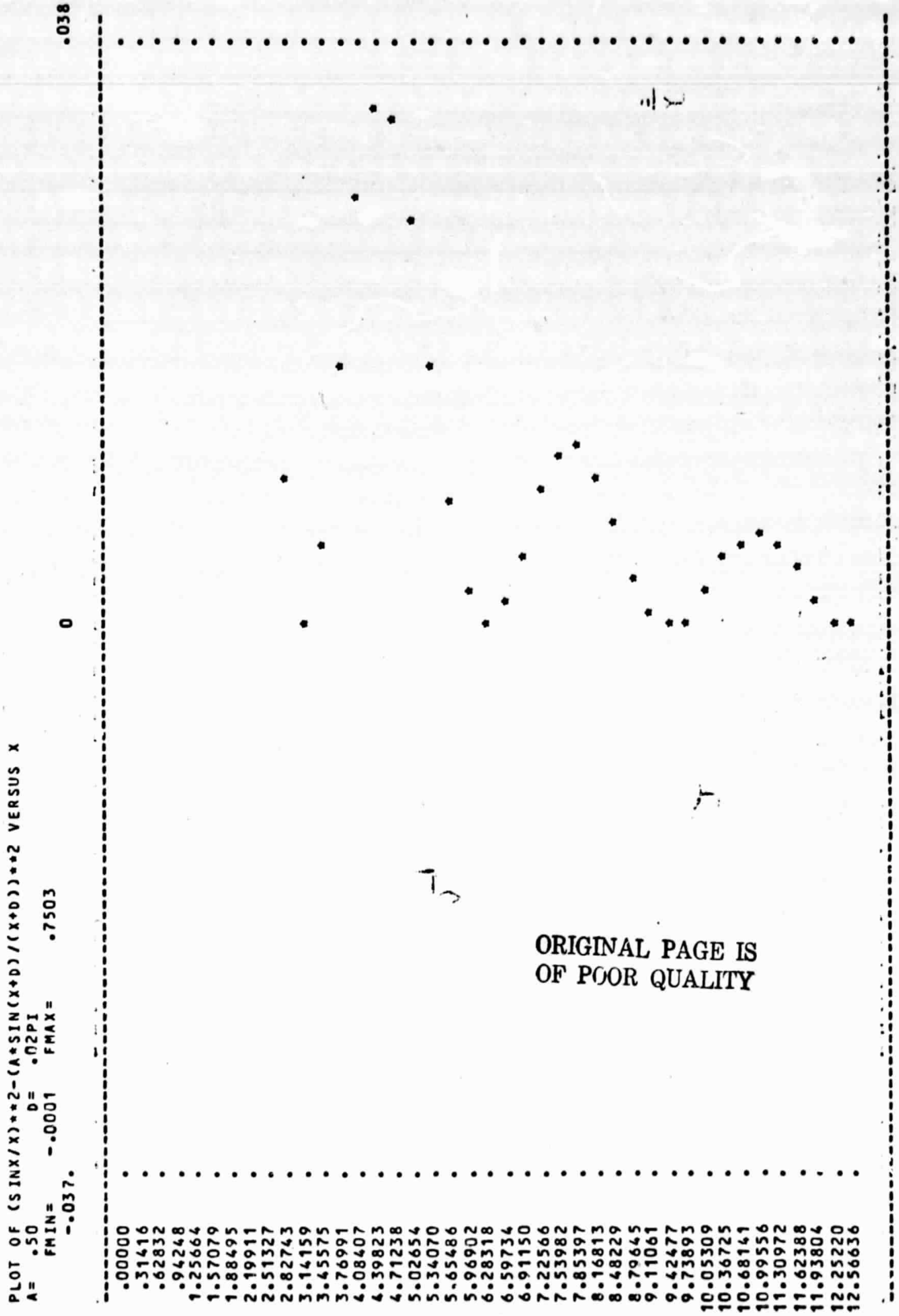
PLOT OF (SINX/X)**2-(A*SIN(X+D)/(X+D))**2 VERSUS X
A= .50 D= .02PI
FMIN= -.0001 FMAX= .7503
-.037
0
.038
.00000
.31416
.62832
.94248
1.25664
1.57079
1.88495
2.19911
2.51327
2.82743
3.14159
3.45575
3.76991
4.08407
4.39823
4.71238
5.02654
5.34070
5.65486
5.96902
6.28318
6.59734
6.91150
7.22566
7.53982
7.85397
8.16813
8.48229
8.79645
9.11061
9.42477
9.73893
10.05309
10.36725
10.68141
10.99556
11.30972
11.62388
11.93804
12.25220
12.56636

Figure 7

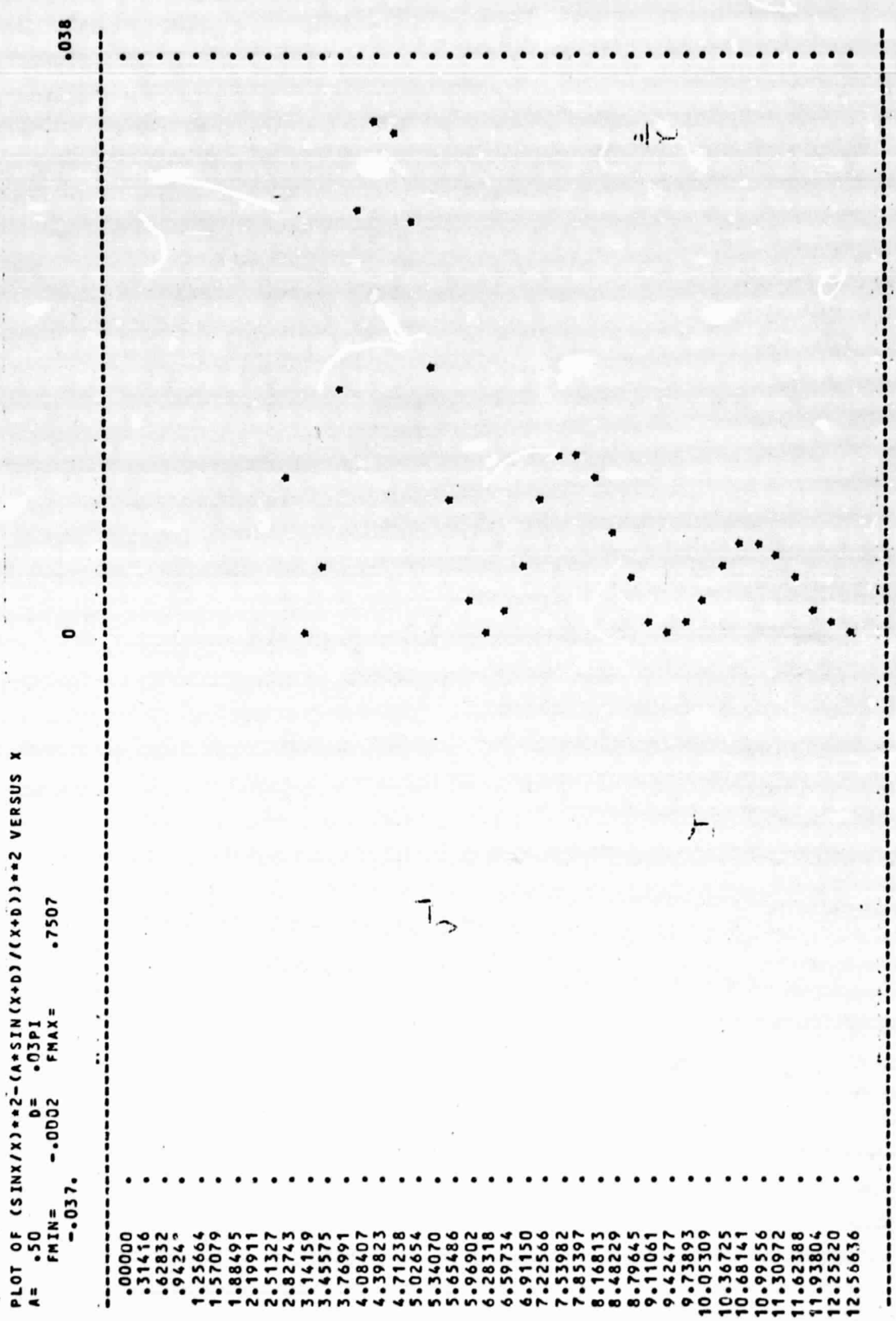
PLOT OF (SINX/X)**2-(A*SIN(X+D)/(X+D))**2 VERSUS X
A= .50 D= .03PI
FMIN= -.0002 FMAX= .7507
-.037. 0 .038
.00000
.31416
.62832
.9424
1.25664
1.57079
1.88495
2.19911
2.51327
2.82743
3.14159
3.45575
3.76991
4.08407
4.39823
4.71238
5.02654
5.34070
5.65486
5.96902
6.28318
6.59734
6.91150
7.22566
7.53982
7.85397
8.16813
8.48229
8.79645
9.11061
9.42477
9.73893
10.05309
10.36725
10.68141
10.99556
11.30972
11.62388
11.93804
12.25220
12.56636

Figure 8

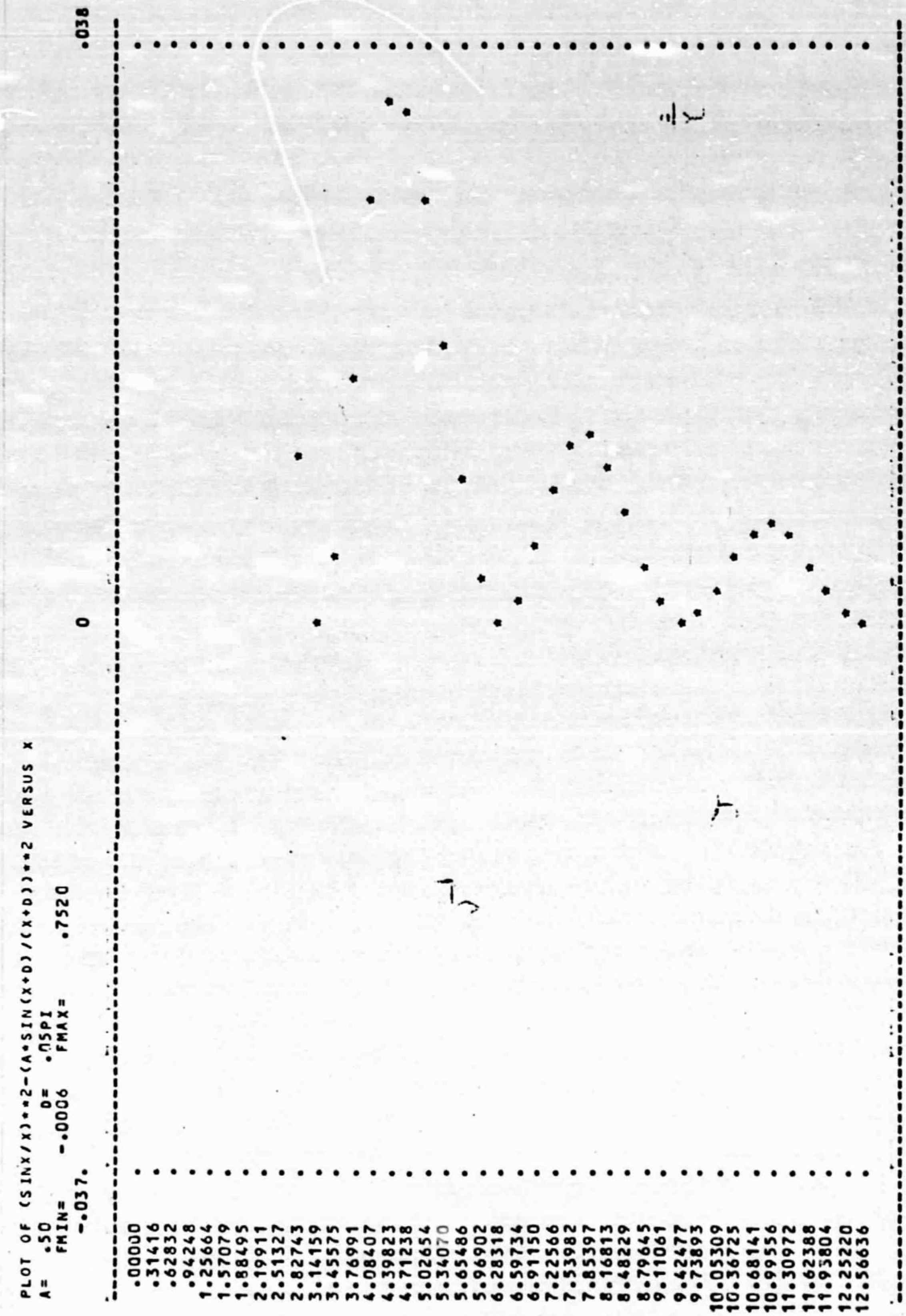
PLOT OF (SINX/X)**2-(A*SIN(X+D)/(X+D))**2 VERSUS X
A= .50 D= .05PI
FMIN= -.0006 FMAX= .7520
-.037.
0
.038
.00000
.31416
.62832
.94248
1.25664
1.57079
1.88495
2.19911
2.51327
2.82743
3.14159
3.45575
3.76991
4.08407
4.39823
4.71238
5.02654
5.34070
5.65486
5.96902
6.28318
6.59734
6.91150
7.22566
7.53982
7.85397
8.16813
8.48229
8.79645
9.11061
9.42477
9.73893
10.05309
10.36725
10.68141
10.99556
11.30972
11.62388
11.93804
12.25220
12.56636

Figure 9

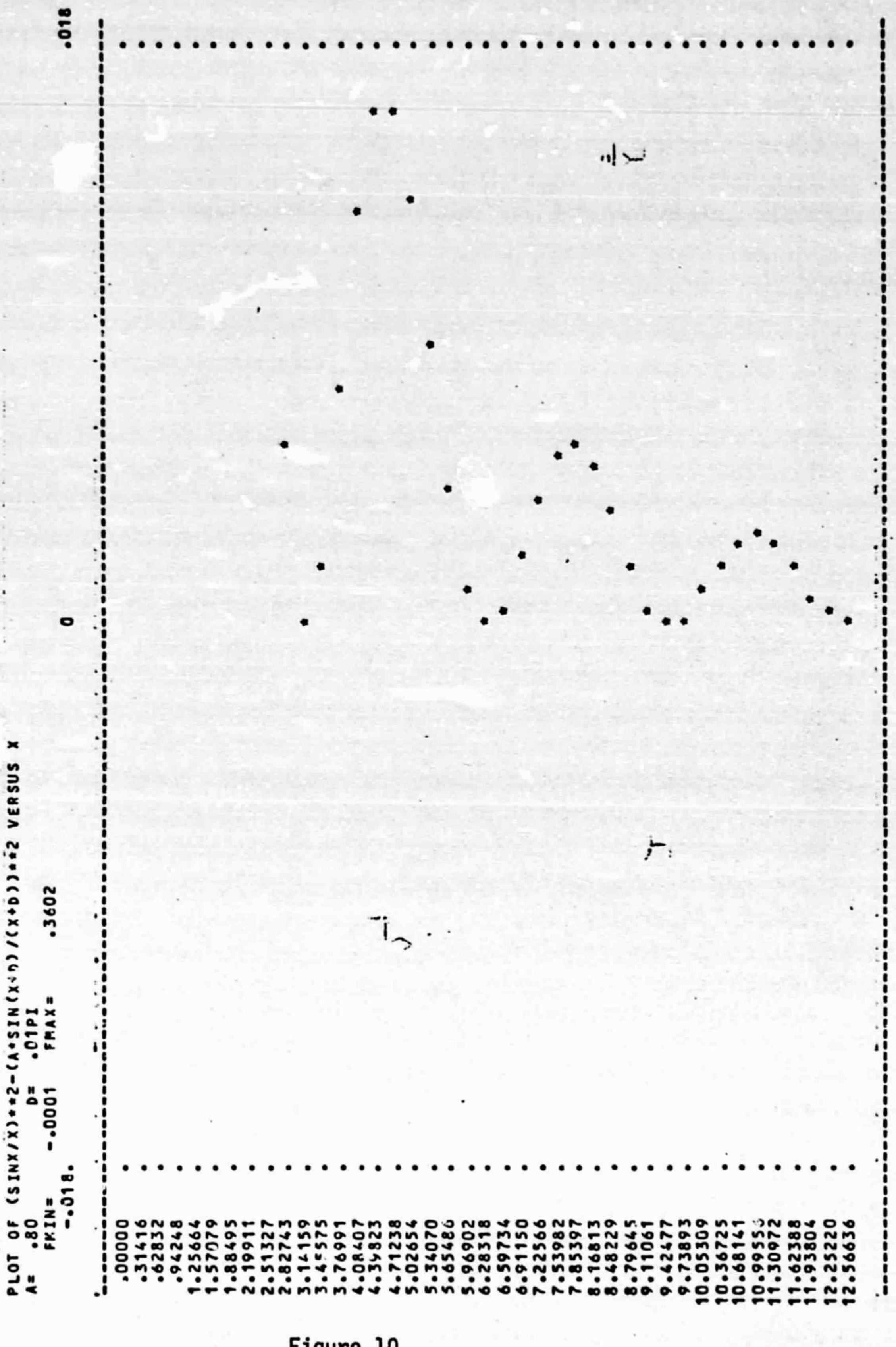
PLOT OF (SINX/X)**2-(A*SIN(X+D)/(X+D))**2 VERSUS X
A= .80 D= .01PI
FMIN= -.0001 FMAX= .3602
-.018
0
.018
.00000
.31416
.62832
.94248
1.25664
1.57079
1.88495
2.19911
2.51327
2.82743
3.14159
3.76991
4.08407
4.71238
5.02654
5.34070
5.96902
6.28318
6.59734
6.91150
7.22566
7.53982
7.85397
8.16813
8.48229
8.79645
9.11061
9.42477
9.73893
10.05309
10.36725
10.68141
11.30972
11.62388
11.93804
12.25220
12.56636

Figure 10

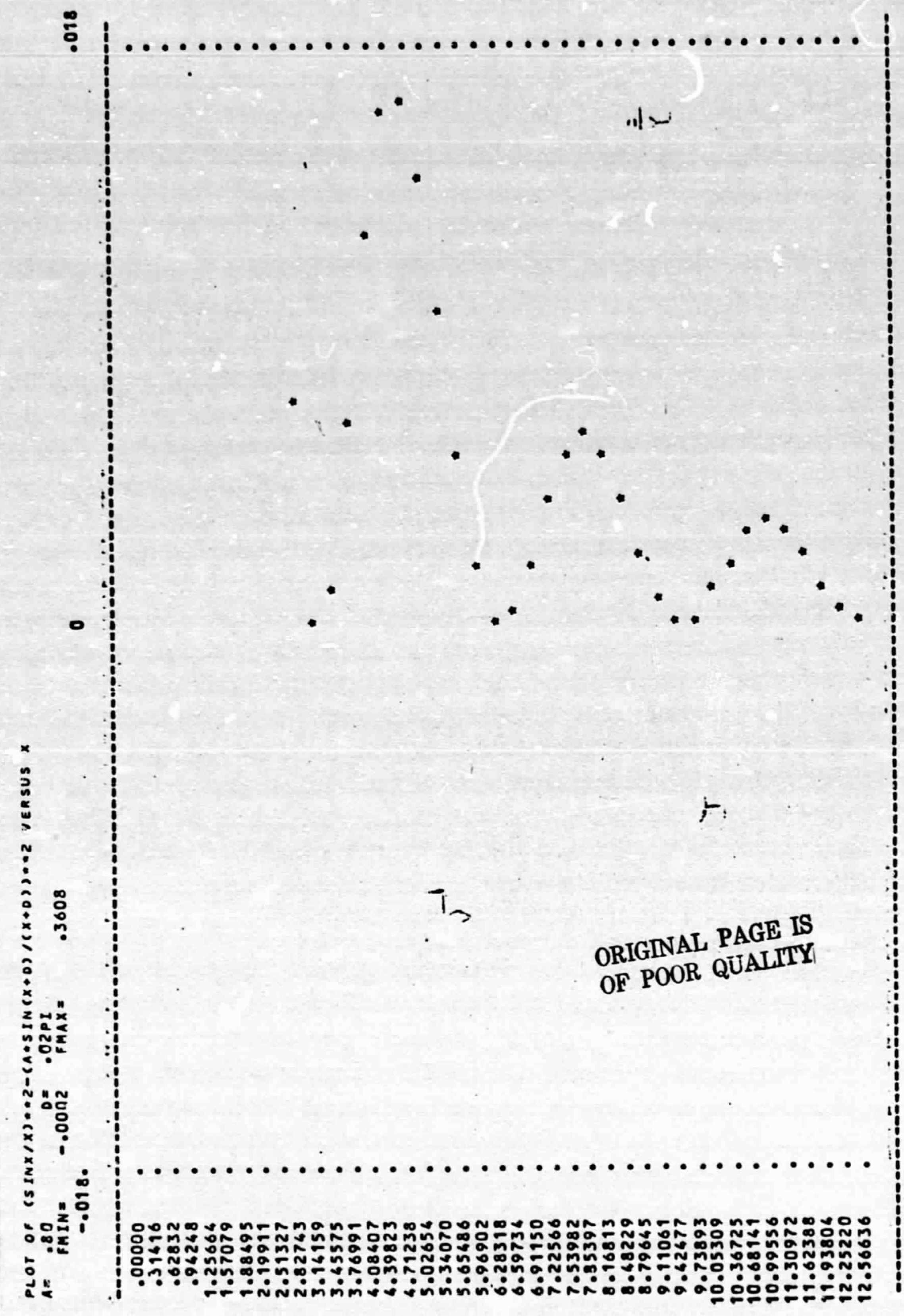
PLOT OF (SINX/X)**2-(A*SIN(X+D)/(X+D))**2 VERSUS X
A= .80 D= .02PI
FMIN= -.0002 FMAX= .3608
-.018
0
.018
.00000
.31416
.62832
.94248
1.25664
1.57079
1.88495
2.19911
2.51327
2.82743
3.14159
3.45575
3.76991
4.08407
4.39823
4.71238
5.02654
5.34070
5.65486
5.96902
6.28318
6.59734
6.91150
7.22566
7.53982
7.85397
8.16813
8.48229
8.79645
9.11061
9.42477
9.73893
10.05309
10.36725
10.68141
10.99556
11.30972
11.62388
11.93804
12.25220
12.56636

Figure 11

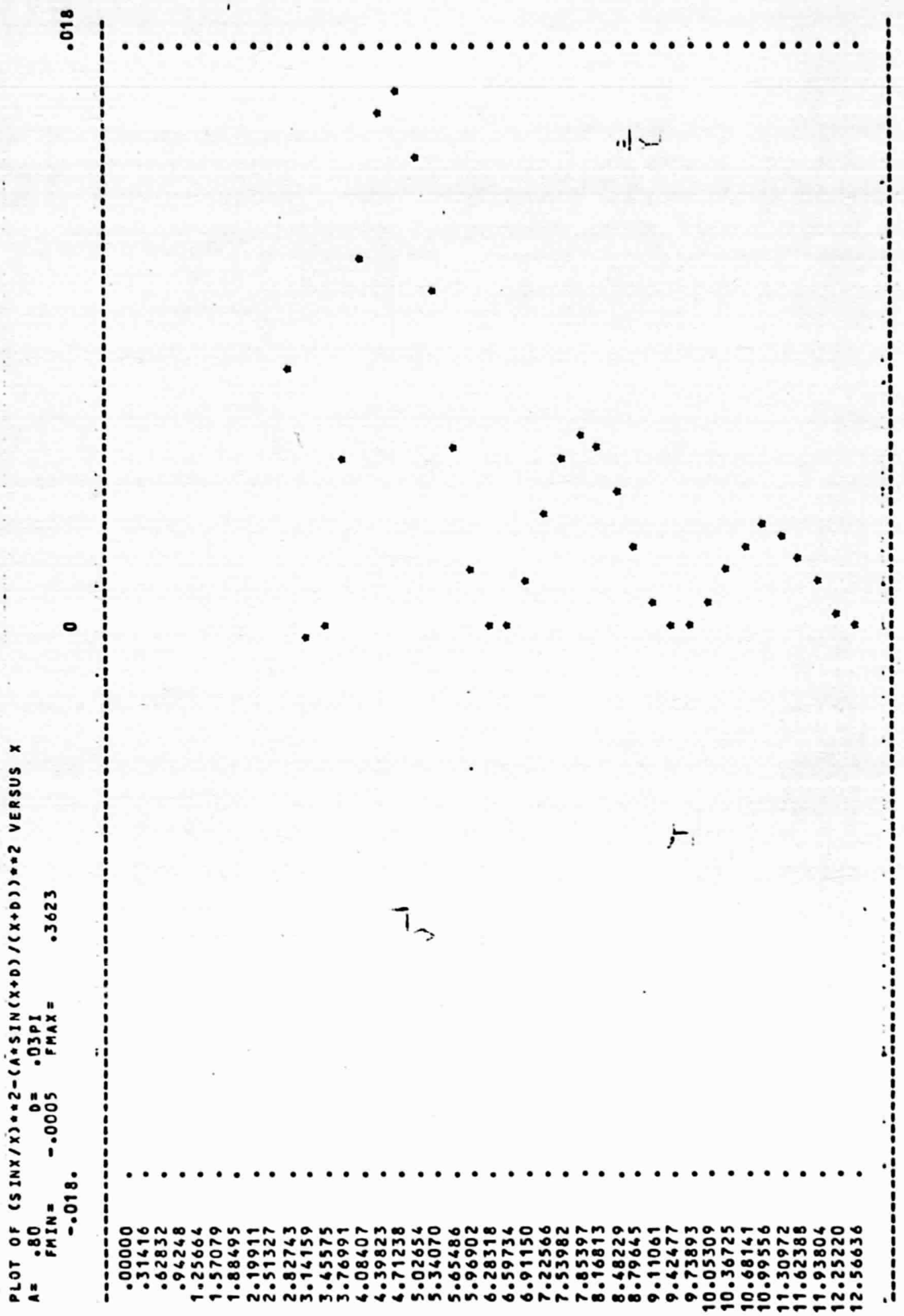
PLOT OF (SINX/X)**2-(A*SIN(X+D)/(X+D))**2 VERSUS X
A= .80 D= .03PI
FMIN= -.0005 FMAX= .3623
-.018
0
.018

Figure 12

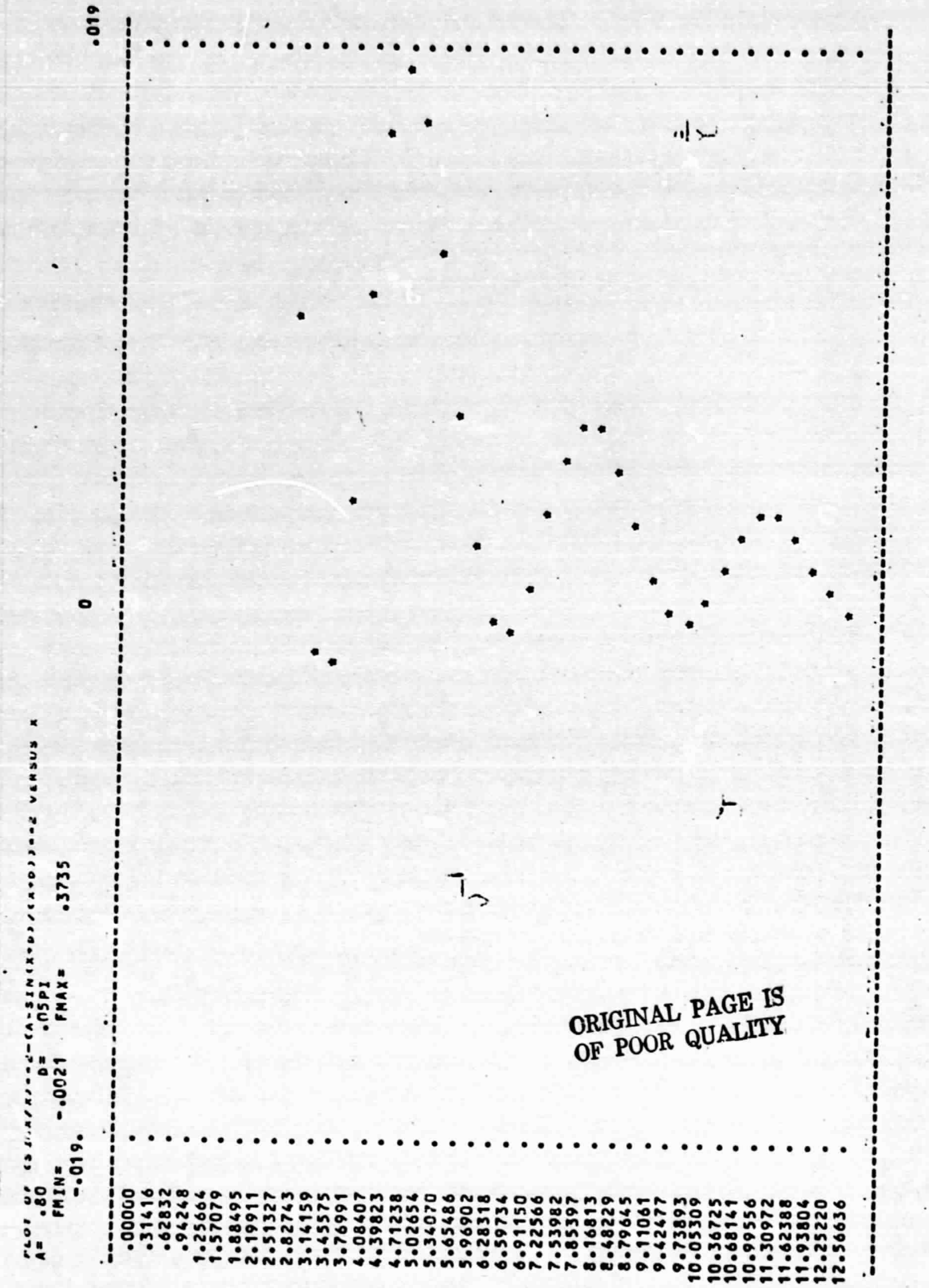
A= .80 D= .05PI
FMIN= -.0021 FMAX= .3735
-.019
0
.019
.00000
.31416
.62832
.94248
1.25664
1.57079
1.88495
2.19911
2.51327
2.82743
3.14159
3.45575
3.76991
4.08407
4.39823
4.71238
5.02654
5.34070
5.65486
5.96902
6.28318
6.59734
6.91150
7.22566
7.53982
7.85397
8.16813
8.48229
8.79645
9.11061
9.42477
9.73893
10.05309
10.36725
10.68141
10.99556
11.30972
11.62388
11.93804
12.25220
12.56636

Figure 13

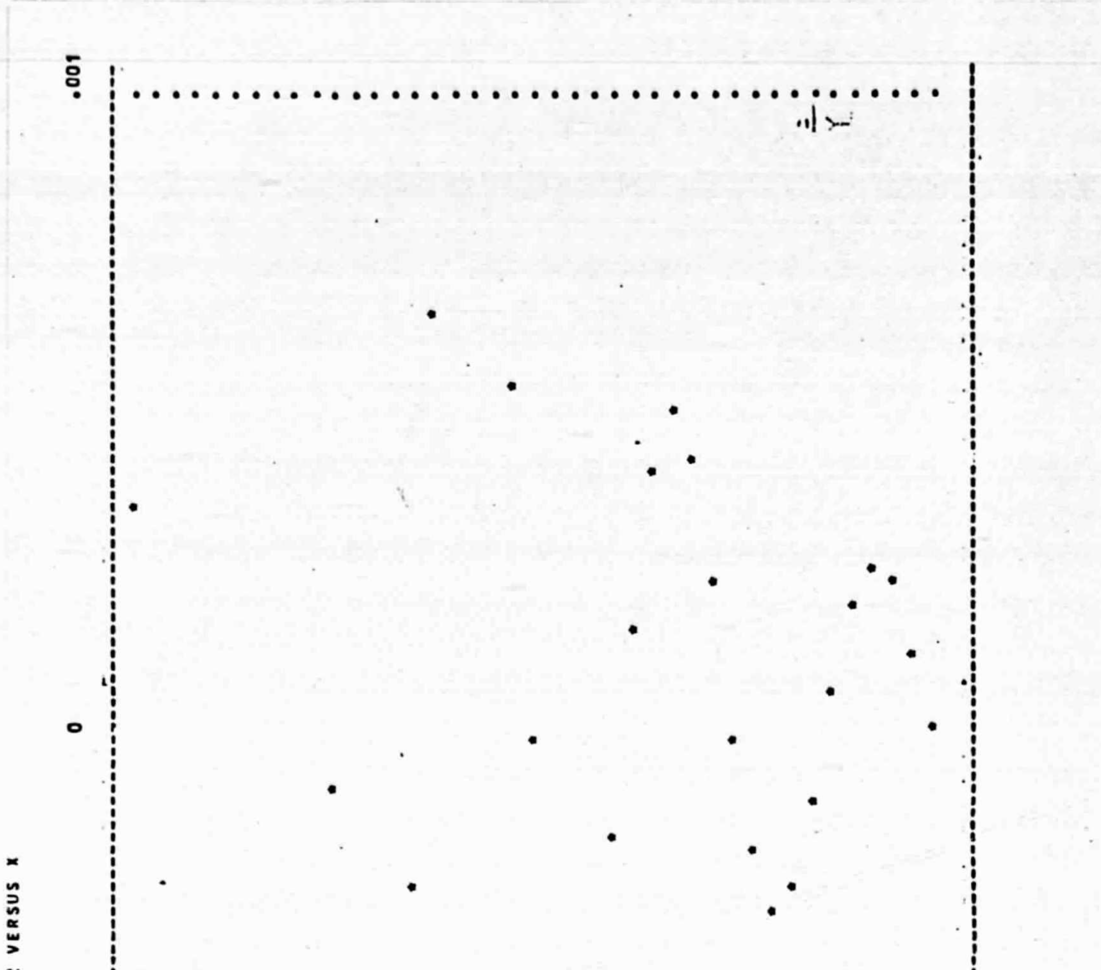
PLOT OF (SINX/X)**2-(A*SIN(X+D)/(X+D))**2 VERSUS X
A= 1.00 D= .01PI
FMIN= -.0017 FMAX= .0170
-.001
0
.001
.00000
.31416
.62832
.94248
1.25664
1.57079
1.88495
2.19911
2.51327
2.82743
3.14159
3.45575
3.76991
4.08407
4.39823
4.71238
5.02654
5.34070
5.65486
5.96902
6.28318
6.59734
6.91150
7.22566
7.53982
7.85397
8.16813
8.48229
8.79645
9.11061
9.42477
9.73893
10.05309
10.36725
10.68141
10.99556
11.30972
11.62388
11.93804
12.25220
12.56636

Figure 14

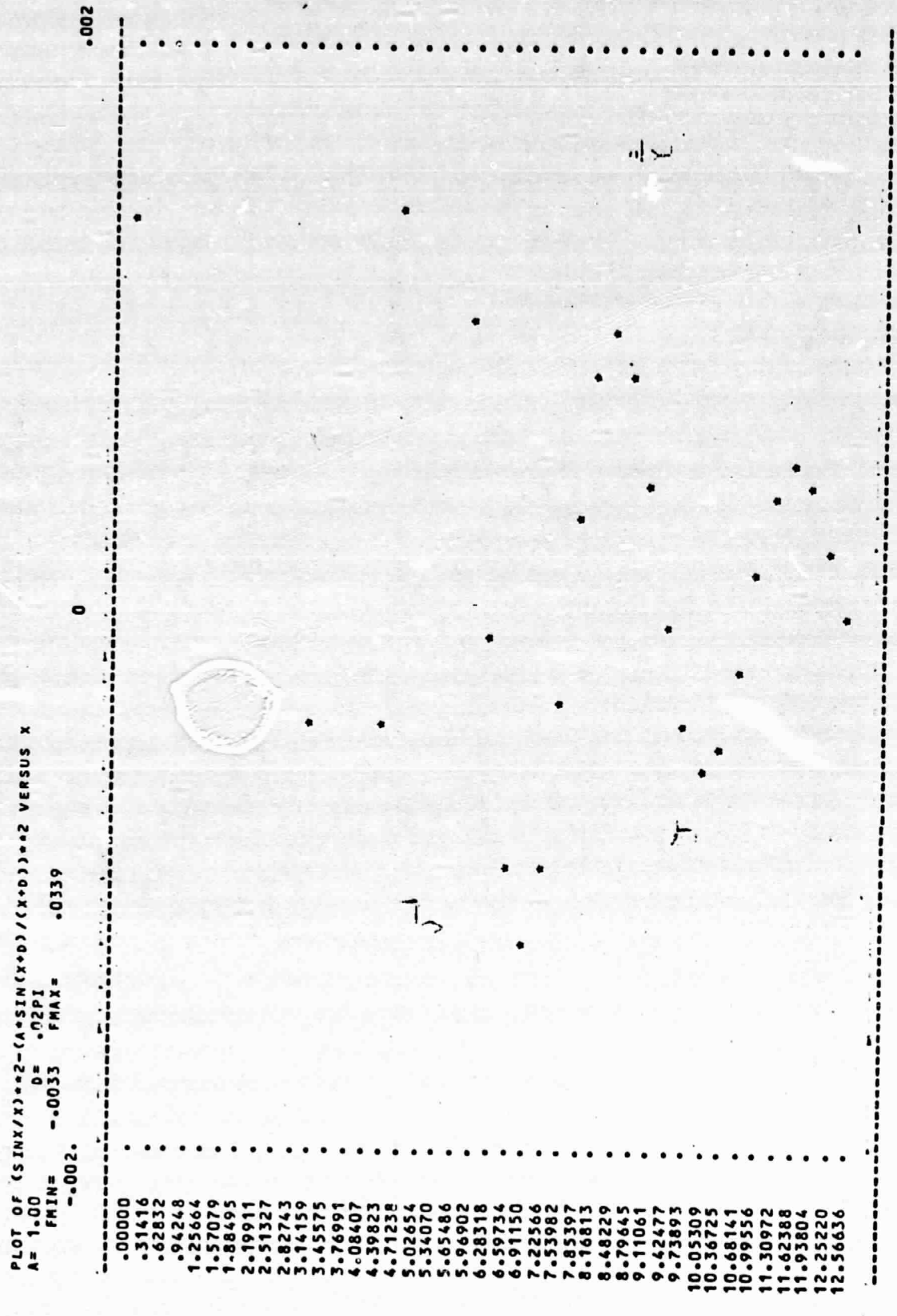

PLOT OF (SINX/X)**2-(A*SIN(X+D)/(X+D))**2 VERSUS X
A= 1.00 D= .02PI
FMIN= -.0033 FMAX= .0339
-.002
0
.002
.00000
.31416
.62832
.94248
1.25664
1.57079
1.88495
2.19911
2.51327
2.82743
3.14159
3.45575
3.76991
4.08407
4.39823
4.71238
5.02654
5.34070
5.65486
5.96902
6.28318
6.59734
6.91150
7.22566
7.53982
7.85397
8.16813
8.48229
8.79645
9.11061
9.42477
9.73893
10.05309
10.36725
10.68141
10.99556
11.30972
11.62388
11.93804
12.25220
12.56636

Figure 15

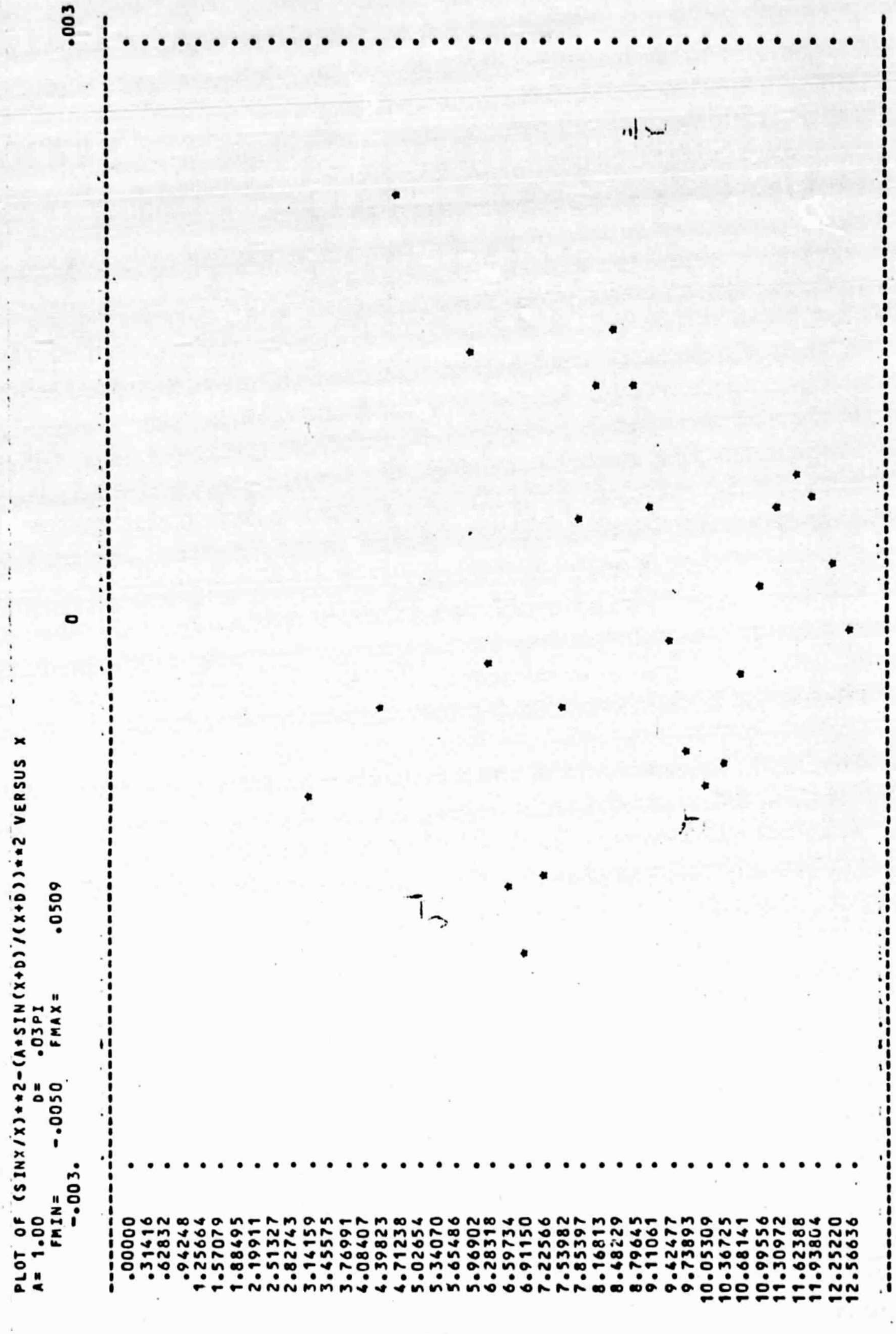

PLOT OF (SINX/X)**2-(A*SIN(X+D)/(X+D))**2 VERSUS X
A= 1.00 D= .03PI
FMIN= -.0050 FMAX= .0509
-.003. 0 .003
.00000
.31416
.62832
.94248
1.25664
1.57079
1.88495
2.19911
2.51327
2.82743
3.14159
3.45575
3.76991
4.08407
4.39823
4.71238
5.02654
5.34070
5.65486
5.96902
6.28318
6.59734
6.91150
7.22566
7.53982
7.85397
8.16813
8.48229
8.79645
9.11061
9.42477
9.73893
10.05309
10.36725
10.68141
10.99556
11.30972
11.62388
11.93804
12.25220
12.56636

Figure 16

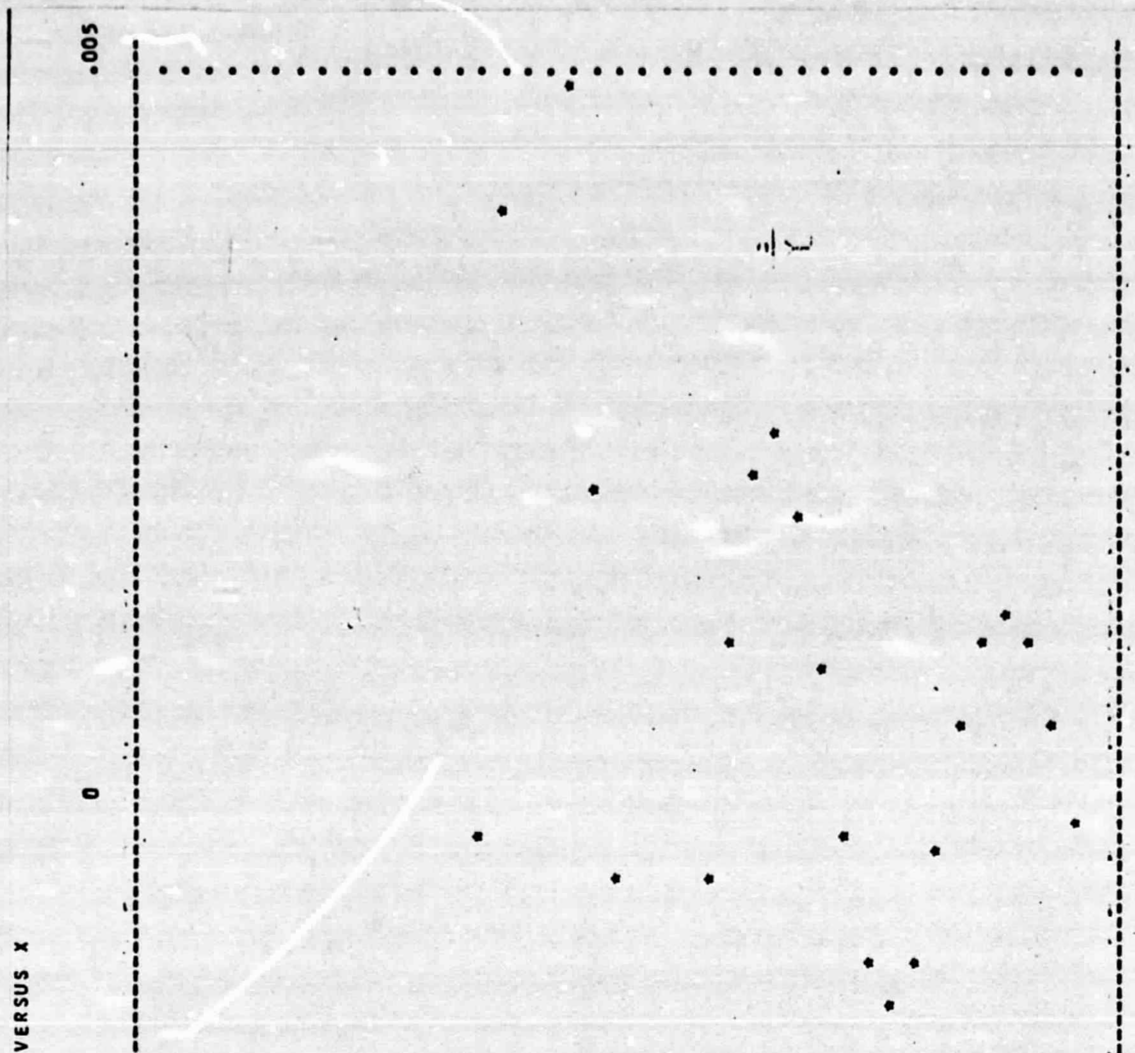
PLOT OF (SINX/X)**2-(A*SIN(X+D)/(X+D))**2 VERSUS X
A= 1.00 D= .05PI
FMIN= -.0081 FMAX= .0847
-.005
0
.005
.00000
.31416
.62832
.94248
1.25664
1.57079
1.88495
2.19911
2.51327
2.82743
3.14159
3.45575
3.76991
4.08407
4.39823
4.71238
5.02654
5.34070
5.65486
5.96902
6.28318
6.59734
6.91150
7.22566
7.53982
7.85397
8.16813
8.48229
8.79645
9.11061
9.42477
9.73893
10.05309
10.36725
10.68141
10.99556
11.30972
11.62388
11.93804
12.25220
12.56636

Figure 17

through 17. In Figures 6 through 9, the parameter A = 0.5, and d = 0.1π, 0.2π, 0.3π, and 0.5π respectively. For the same series of value of the parameter d, Figures 10 through 13 are with A = 0.8; and Figures 14 through 17 are with A = 1.0. Figures 6 through 17 clearly demonstrated that slight misalignment and/or misadjustment of the intensity of two simple fringe patterns will give rise to another fringe pattern which is just as complicated in relative fringe contrast as the original fringe pattern. The computer-simulated result implies that when the holographic interference fringe patterns of real double-exposure holograms or real-time holograms are combined without any precise knowledge of the phase and amplitude parameters, uninterpretable and confusing result will easily occur.

The outputs of computer programs 3 and 4 showing the fringe subtractions of the Airy ring fringe patterns demonstrated the same fact; further reinforced the correctness that the idea of fringe subtraction is not practical for the HNDT work.

Based on the above conclusion, a new approach was searched for the purpose of achieving the original goal to improve the data reduction process in a HNDT system. A technique called the phase-modulated triple-exposure holographic interferometric method was found. This technique will be discussed in the next section.

III. Phase-modulated Triple-exposure Holographic Interferometry

The technique is based on D. Gabor et al's[3] suggestion that complex addition of images or the interference patterns is a type of "true" optical filtering process. Complex image addition or subtraction may be called an "optical image synthesis" process. We shall utilize this concept together with a phase shift operation during a triple-exposure process to identify the no-motion fringe; in the meantime, it is expected that the direction of the object's displacement may also be determined.

The intensity of the fringes in holographic interferometry is proportional to the square of the characteristic function. In general, it is necessary to solve the equation

$$I(r) = I_0(r) \left\{ \frac{1}{T} \int_0^T \exp\left[j\, \phi\, (r, t)\right] dt \right\}^2 , \qquad (6)$$

where $I_0(r)$ denotes the intensity at point r as reconstructed from an ordinary single-exposure hologram, T, the exposure time, and $\phi\ (r, t)$ the phase of the object beam relative to the reference beam.

We shall assume that in general, the loading of the object causes the phase $\phi\ (r, t)$ to vary according to

$$\phi(r, t) = \begin{cases} \phi_1(r) & ; \quad t < t_3 , \\ f(r, t) & ; \quad t_3 < t < t_6 , \\ \phi_2(r) & ; \quad t > t_6 . \end{cases} \qquad (7)$$

Or,

$$\begin{aligned} \phi(r, t) = {} & \phi_1(r)\, [u(t) - u(t - t_3)] \\ & + f(r, t)\, [u(t - t_3) - u(t - t_6)] \\ & + \phi_2(r)\, u(t - t_6) , \end{aligned} \qquad (8)$$

where u(t) is the unit-step function defined by

$$\begin{aligned} u(t) &= 1 , \quad t \geq 0 \\ &= 0 , \quad t < 0 . \end{aligned} \qquad (9)$$

The phase function $\phi(r, t)$ is plotted and shown in Figure 18. In Figure 18, the broadened parts of the curve show the time intervals while exposures

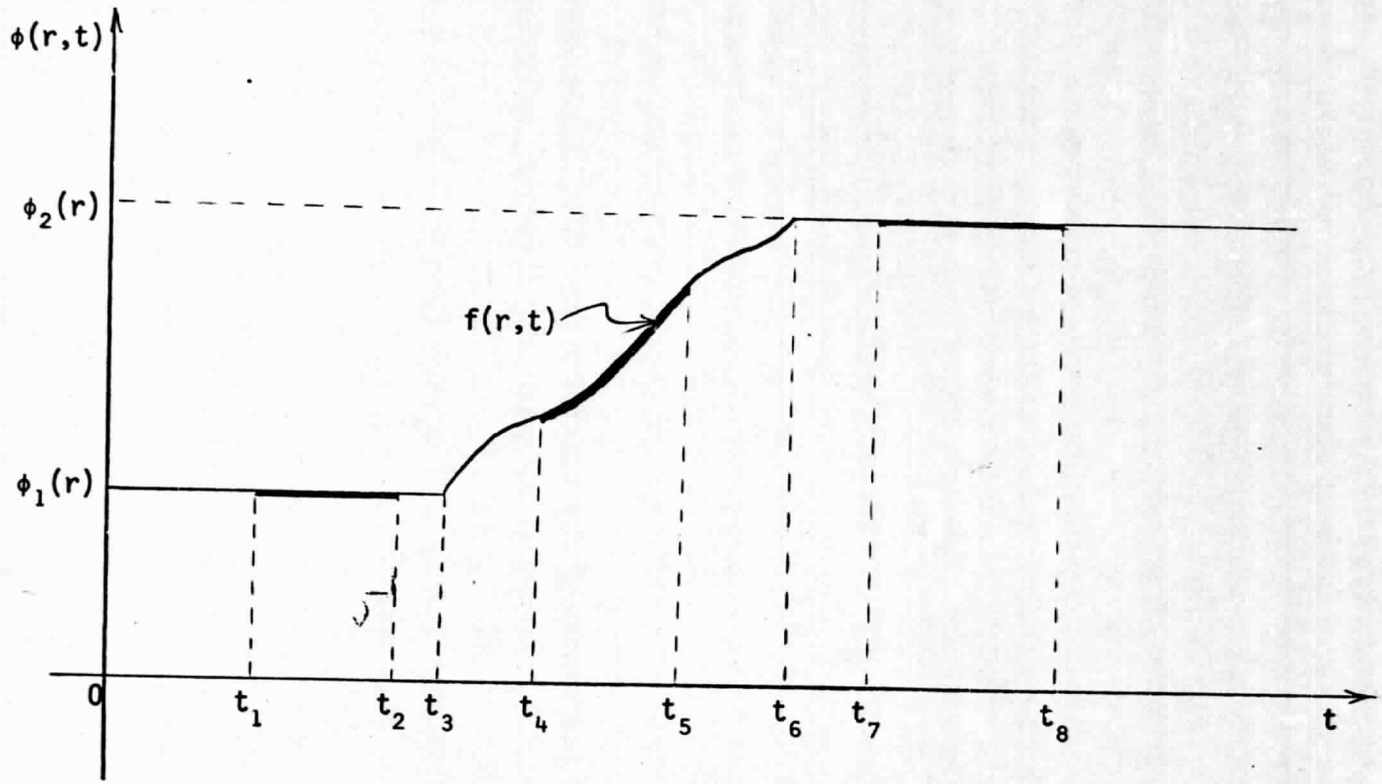

Figure 18. Phase function $\phi(r,t)$ versus t due to loading of the object.

ORIGINAL PAGE IS
OF POOR QUALITY

of the hologram are made. These time intervals are between t_1 and t_2; t_4 and t_5; and t_7 and t_8. Ordinary double-exposure holograms are made usually between t_1 and t_2 ; and t_7 and t_8. A third exposure between t_4 and t_5 is added in the present case. This additional exposure during the loading process is the key to the triple exposure technique.

According to the exposure scheme shown in Fig. 18, Eq. (6) may be written as

$$I(r) = I_0(r) \left\{ \frac{1}{T}\left(\int_{t_1}^{t_2} \exp[j\phi_1(r)]\, dt + \int_{t_4}^{t_5} \exp[jf(r,t)]\, dt + \int_{t_7}^{t_8} \exp[j\phi_2(r)]\, dt \right) \right\}^2 , \tag{10}$$

where if we define

$$\begin{aligned} t_2 - t_1 &\equiv T_1 \\ t_5 - t_4 &\equiv T_2 \\ t_8 - t_7 &\equiv T_3 \quad , \end{aligned} \tag{11}$$

then in Eq. (10)

$$T = T_1 + T_2 + T_3 \tag{12}$$

In addition to the third exposure, we may also introduce various constant phase factors by inserting phase-plates into the laser beam during the second and their exposures. If these phase factors are denoted by α and β respectively, then Eq. (10) becomes

$$I(r) = I_0(r) \left\{ \frac{1}{T} \left(\int_{t_1}^{t_2} \exp[j\phi_1(r)]\, dt \right.\right.$$

$$+ \int_{t_4}^{t_5} \exp[jf(r,t) + j\alpha]\, dt$$

$$\left.\left. + \int_{t_7}^{t_8} \exp[j\phi_2(r) + j\beta]\, dt \right\}^2 . \qquad (13)$$

The above equation represents the basic principle for the phase-modulated triple-exposure holographic interferometry.

To illustrate the effect of Eq. (13), we shall present an example below. The function f(r,t) in Eqs. (7) and (8) is generally unknown, and position dependent, and therefore is subject to one's conjucture. We shall assume, for simplicity, that it is space-independent and varies linearly with respect to time. In addition, we shall assume that the exposure during the loading process begins while the loading begins, and ends at the end of the loading period. Consequently, the phase function becomes

$$\phi(r,t) = \begin{cases} \phi(r); & t < t_2 , \\ [(t - t_1)/(t_2 - t_1)]\, \Delta\phi(r) ; & t_2 < t < t_3 , \\ \phi(r) + \Delta\phi(r) ; & t > t_3 . \end{cases} \qquad (14)$$

Equation (14) is plotted and shown in Fig. 19. The three exposures are now between time periods t_1, t_2; t_2, t_3; and t_3, t_4.

For simplicity, we shall let

$$\begin{aligned} t_2 - t_1 &= T_1 , \\ t_3 - t_2 &= T_2 , \qquad (15) \\ \text{and} \quad t_4 - t_3 &= T_1 , \end{aligned}$$

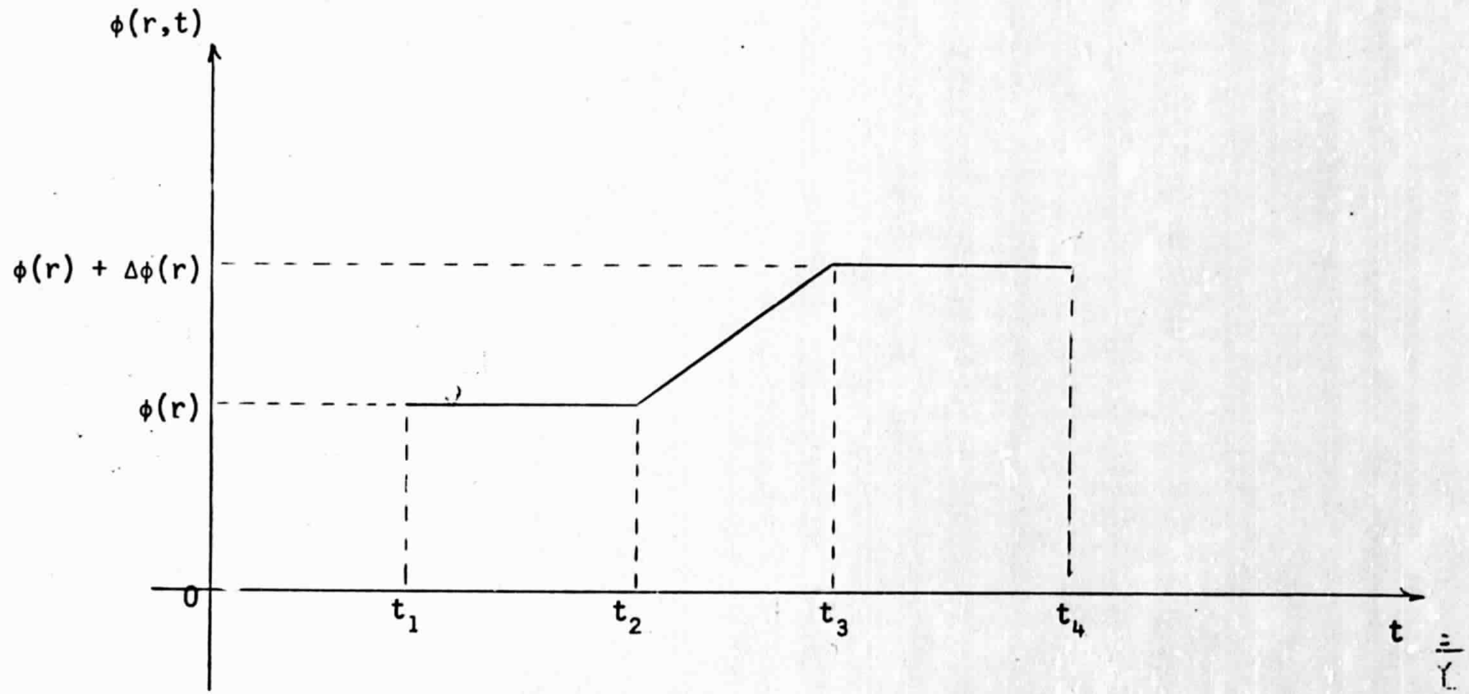

Figure 19. Phase function $\phi(r,t)$ versus t for the example.

where $$T = 2T_1 + T_2$$

By letting $\alpha = \beta = 0$ and substituting Eq. (14) into Eq. (13), one obtains[4-6]

$$I(r) = [I_0(r)/T^2] [2T_1 \cos X + T_2 (\sin X/X)]^2 \qquad (16)$$

If instead $\alpha = \beta = 0$, we have $\alpha = 0$ but $\beta = \pi$, Eq. (16) should be

$$I(r) = [I_0(r)/T^2] [2T_1 \sin X)^2 + (T_2 \sin X/X)^2] \quad ; \qquad (17)$$

and for $\alpha = \pi/2$, $\beta = \pi$, and $\Delta\phi \rightarrow -\Delta\phi$, Eq. (16) becomes

$$I(r) = [I_0(r)/T^2] [2T_1 \sin x - T_2 (\sin X/X)]^2. \qquad (18)$$

The variable X in Eqs. (16) through (18) is defined by

$$X = \frac{\Delta\phi}{2} \quad . \qquad (19)$$

Equations (17) and (18) can be normalized respectively that yields respectively

$$\bar{I}(r) = \sin^2 X + D^2 \sin^2 X/X^2 \quad , \qquad (20)$$

and

$$\bar{I}(r) = [\sin X - D \sin X/X]^2 \quad , \qquad (21)$$

where

$$\bar{I}(r) = T^2 I(r)/[4T_1{}^2 I_0(r)] \quad , \qquad (22)$$

and

$$D = T_2/(2T_1) \quad . \qquad (23)$$

Computer programs have been written to calculate and plot Eqs. (20) and (21). Corresponding to Eq. (20), Figures 20 through 23 show the variation of the normalized intensity in the reconstructed image against the phase change $X = \Delta\phi/2$ for D = 1, 2, 3, and 4 respectively. It is clear that all dark fringes occur at an interval of 2π for all values of D. The zero-order fringe is reconstructed much brighter than higher order fringes as shown in Figures 21 through 23 for $D \geq 2$. Hence, it may be concluded that the zero-order fringe due to no-motion can be identified by having a change of phase of π in one of the beam for the final exposure and a long intermediate

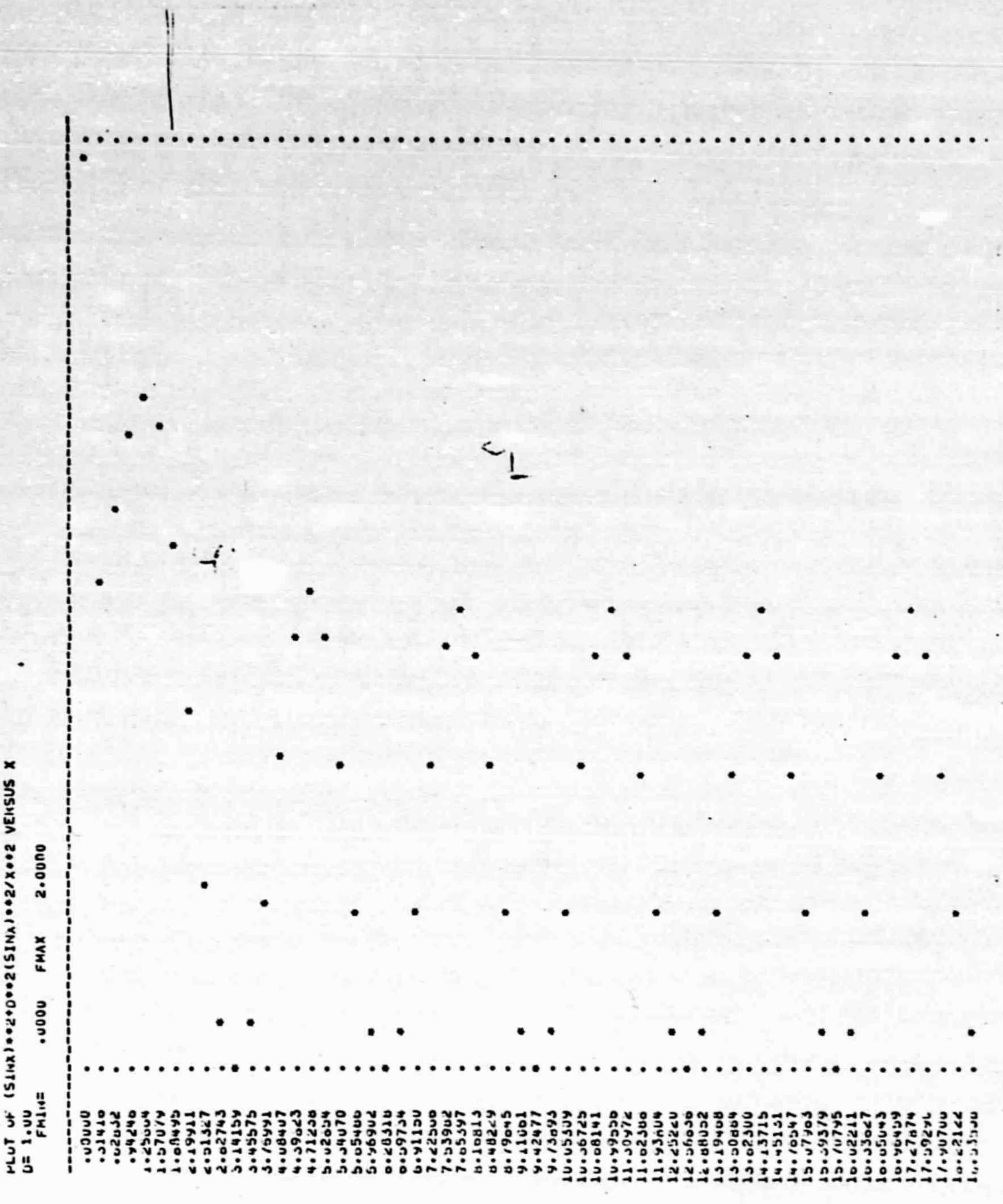

Figure 20

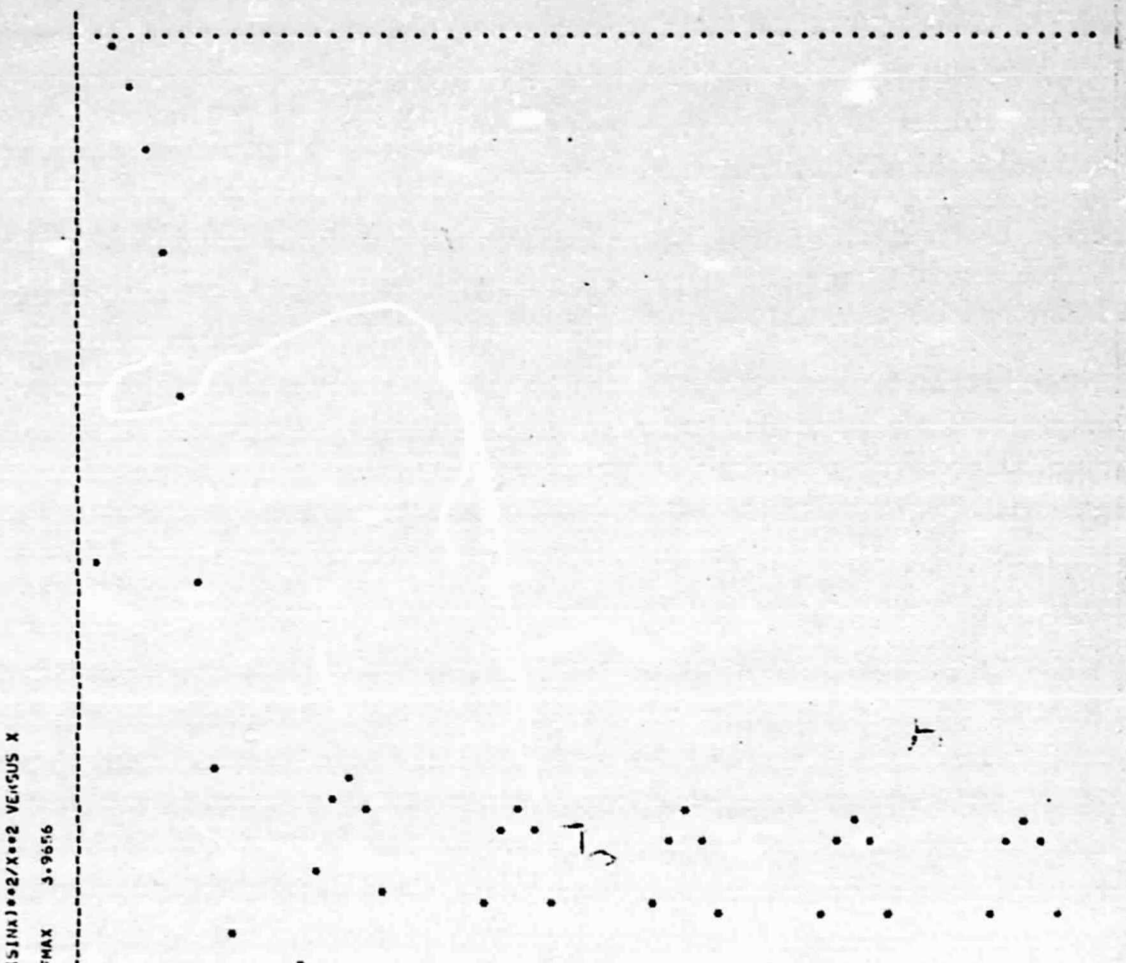

Figure 21

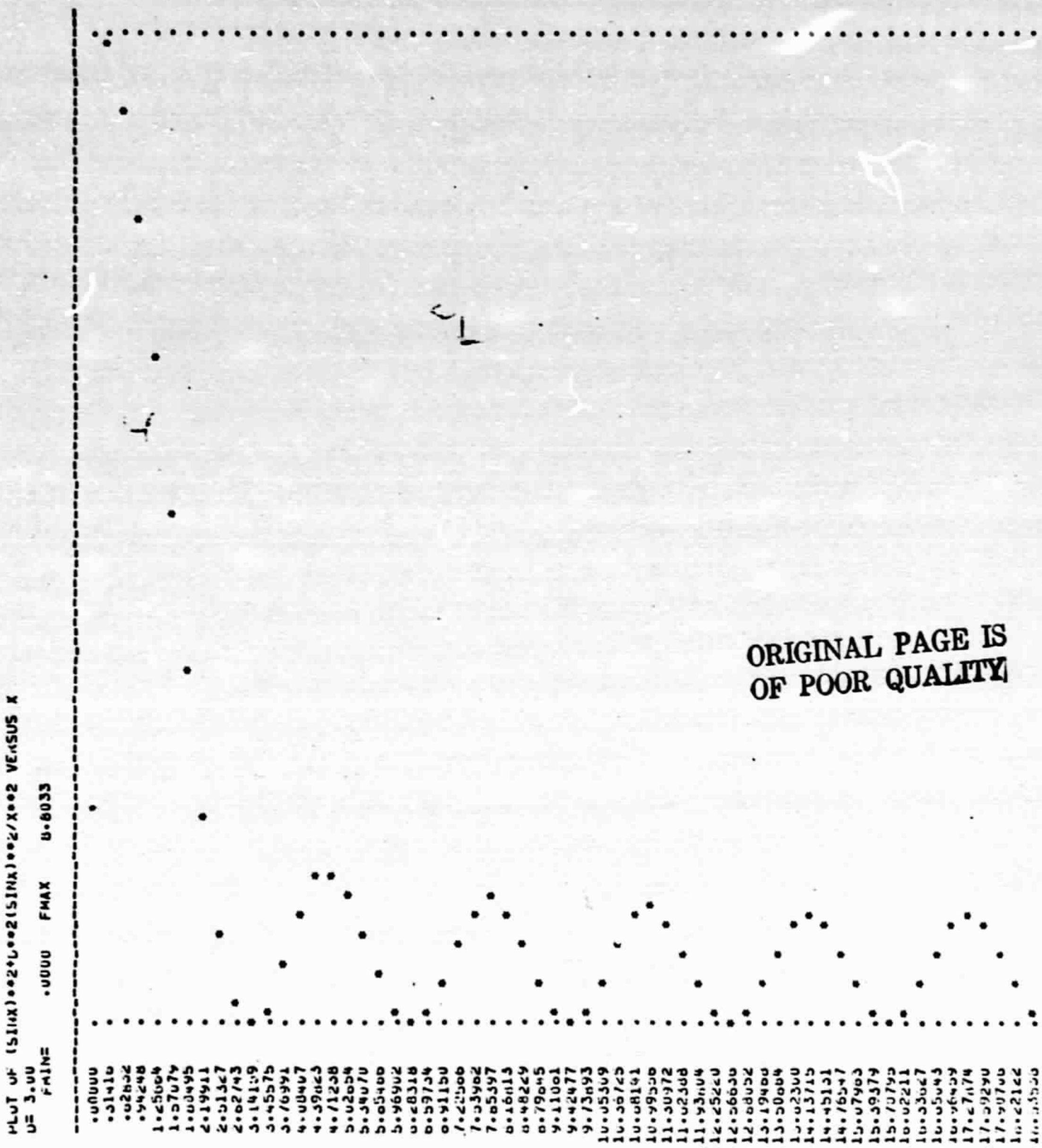

Figure 22

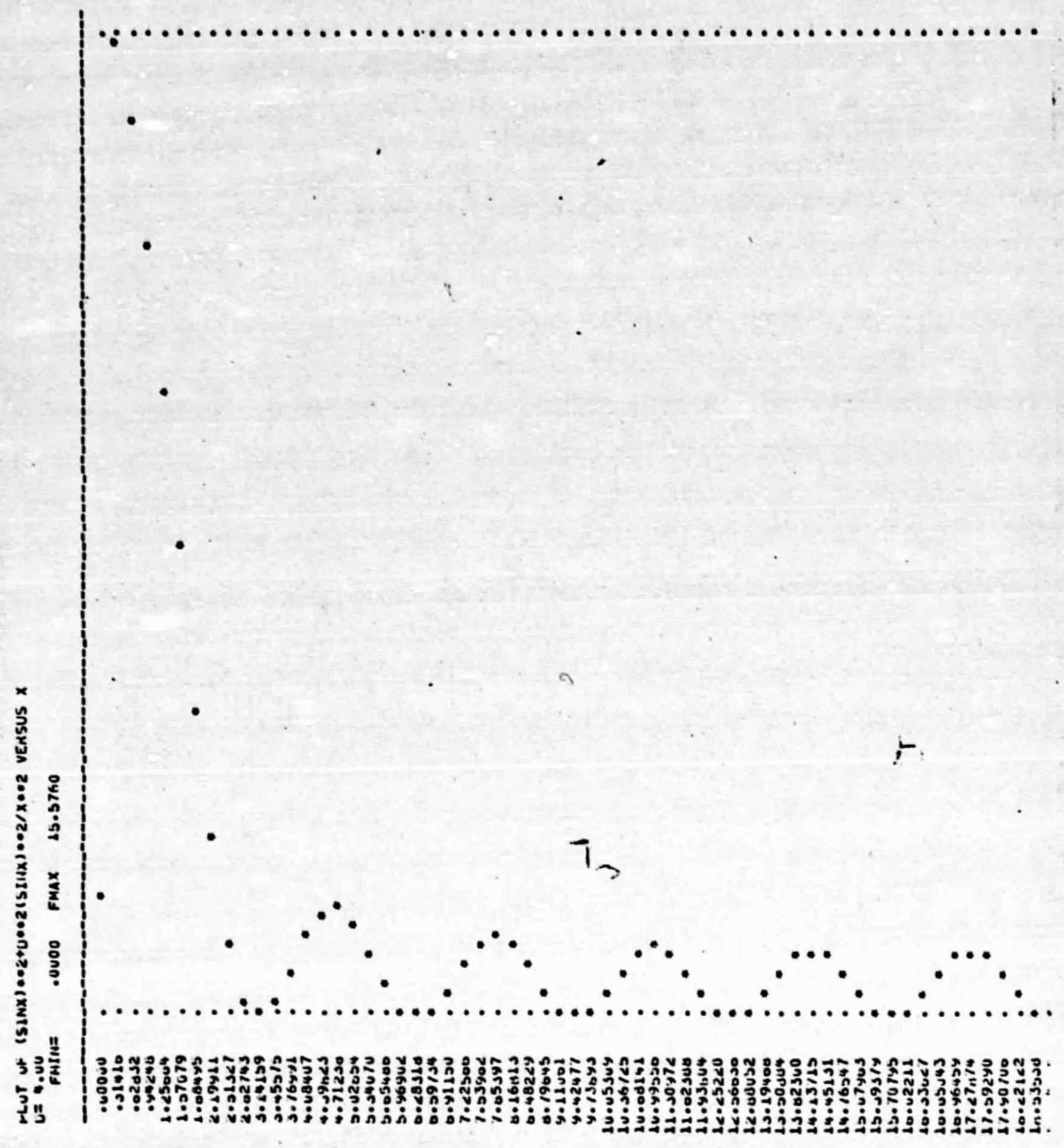

Figure 23

exposure during the loading process such that $D = T_2/(2T_1) \geq 2$. This technique, however, will not detect the direction of motion. The detection of the direction of motion is discussed below.

Corresponding to Eq. (21), Figs. 24 through 27 show the normalized intensity for D = 1, 2, 3, and 4 respectively versus the phase change X. Again, it may be noted that all dark fringes occur at an interval of 2π for all D, and the zero-order fringe is much more intense compared with the rest. For the case where $\Delta\phi$ is negative, the intensity of bright fringes gradually increases with the increase of the fringe order. An increase of 3 times from the first-order fringe to the 5th-order fringe is visible for D = 1; and about 2 times for D = 2. For the case where ϕ is positive (plots not shown), the intensity of bright fringes decreases with the increase of the fringe order. Since the sign of the phase $\Delta\phi$ is correlated to the direction of motion, this characteristic of the fringes enables one to discern the positive direction of motion from the negative direction of motion of the object at position r.

The computer programs given the above plots are listed as program 5 and program 6 in Appendix A.

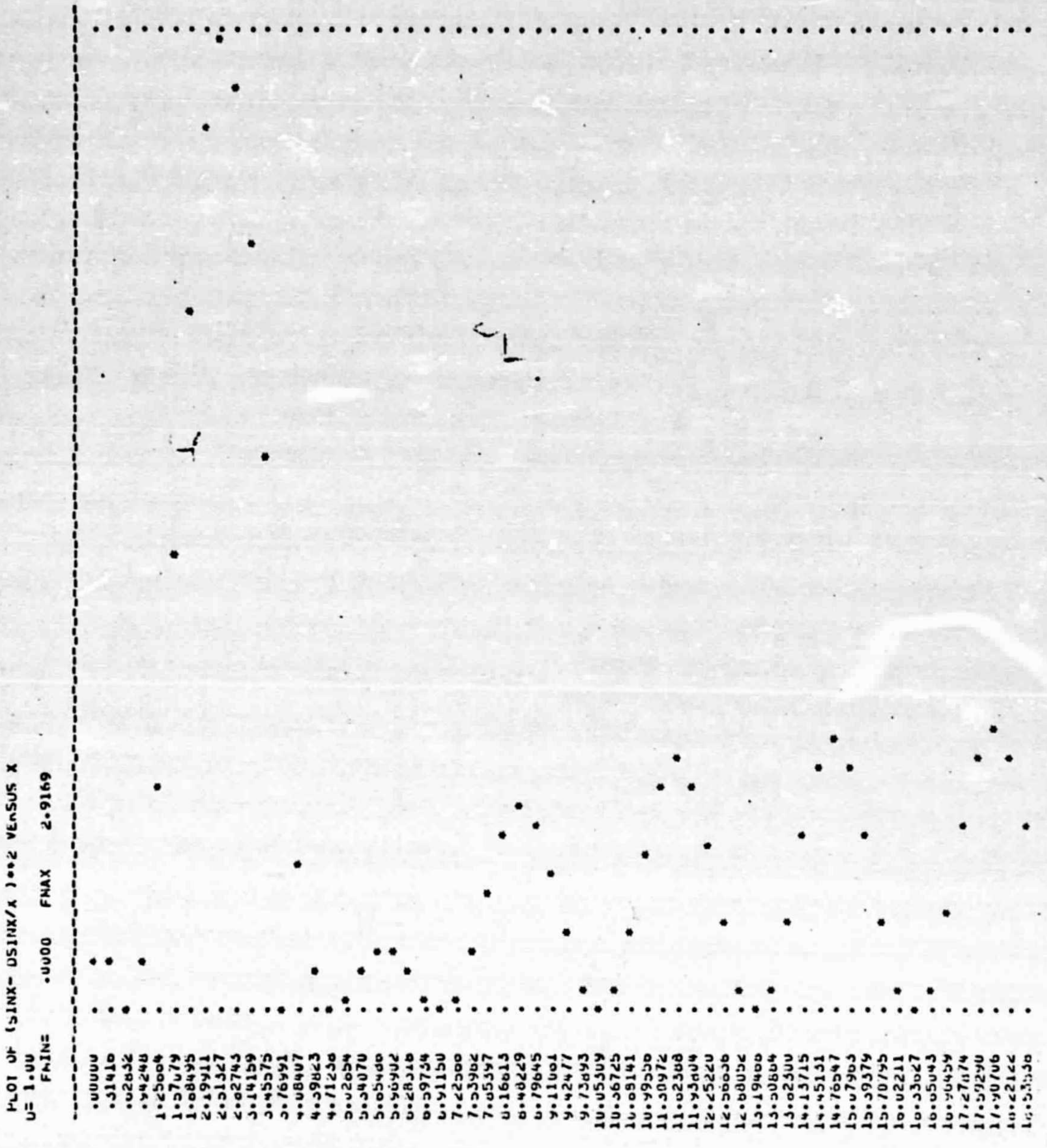

Figure 24

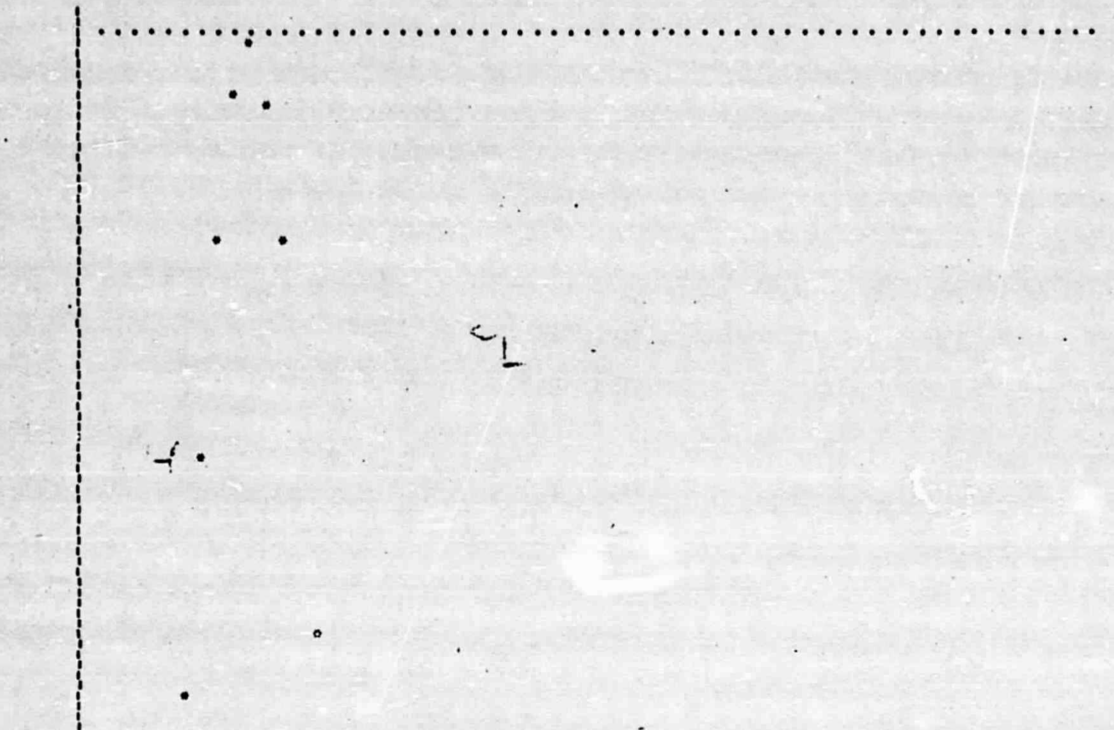

Figure 25

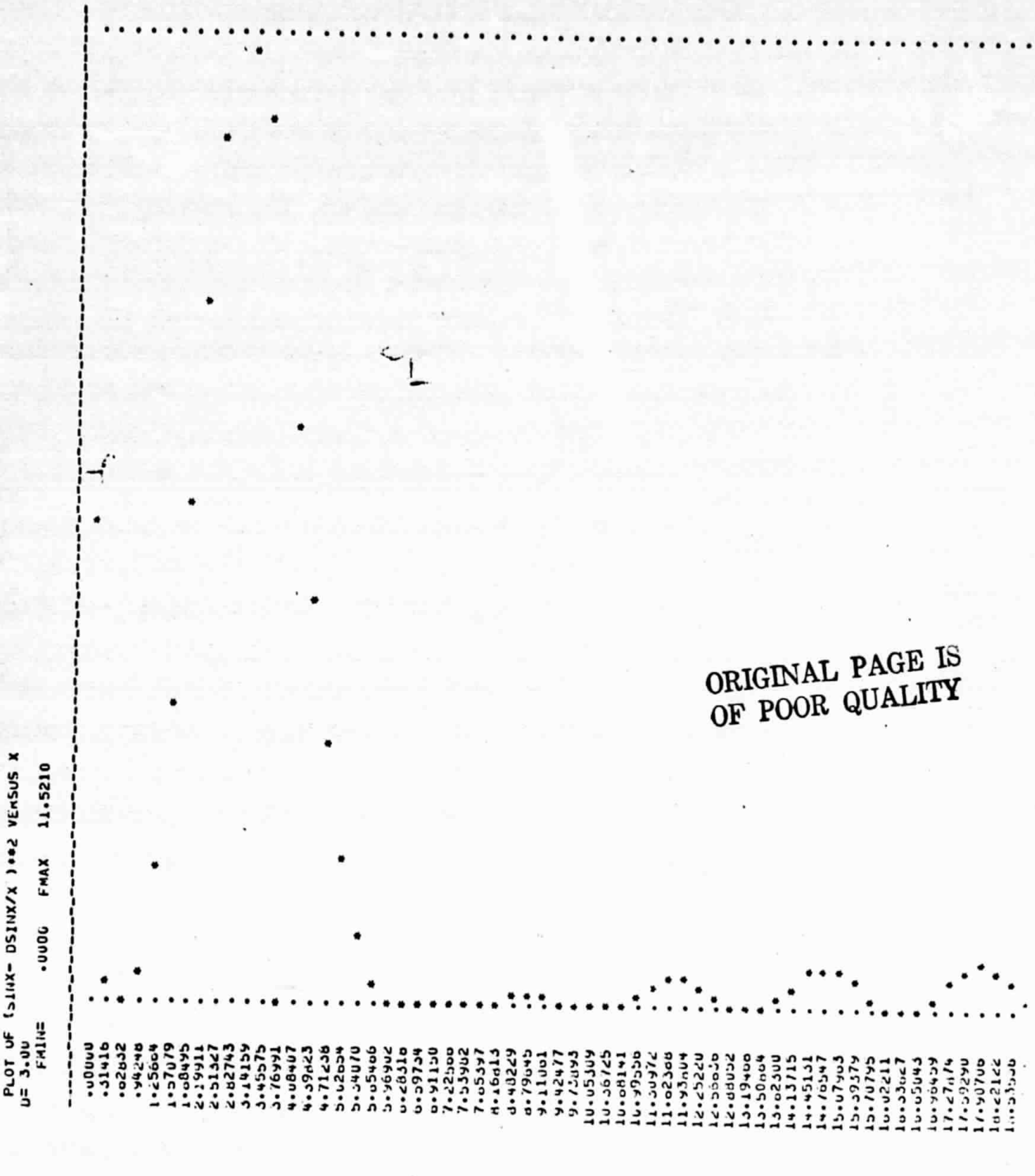

Figure 26

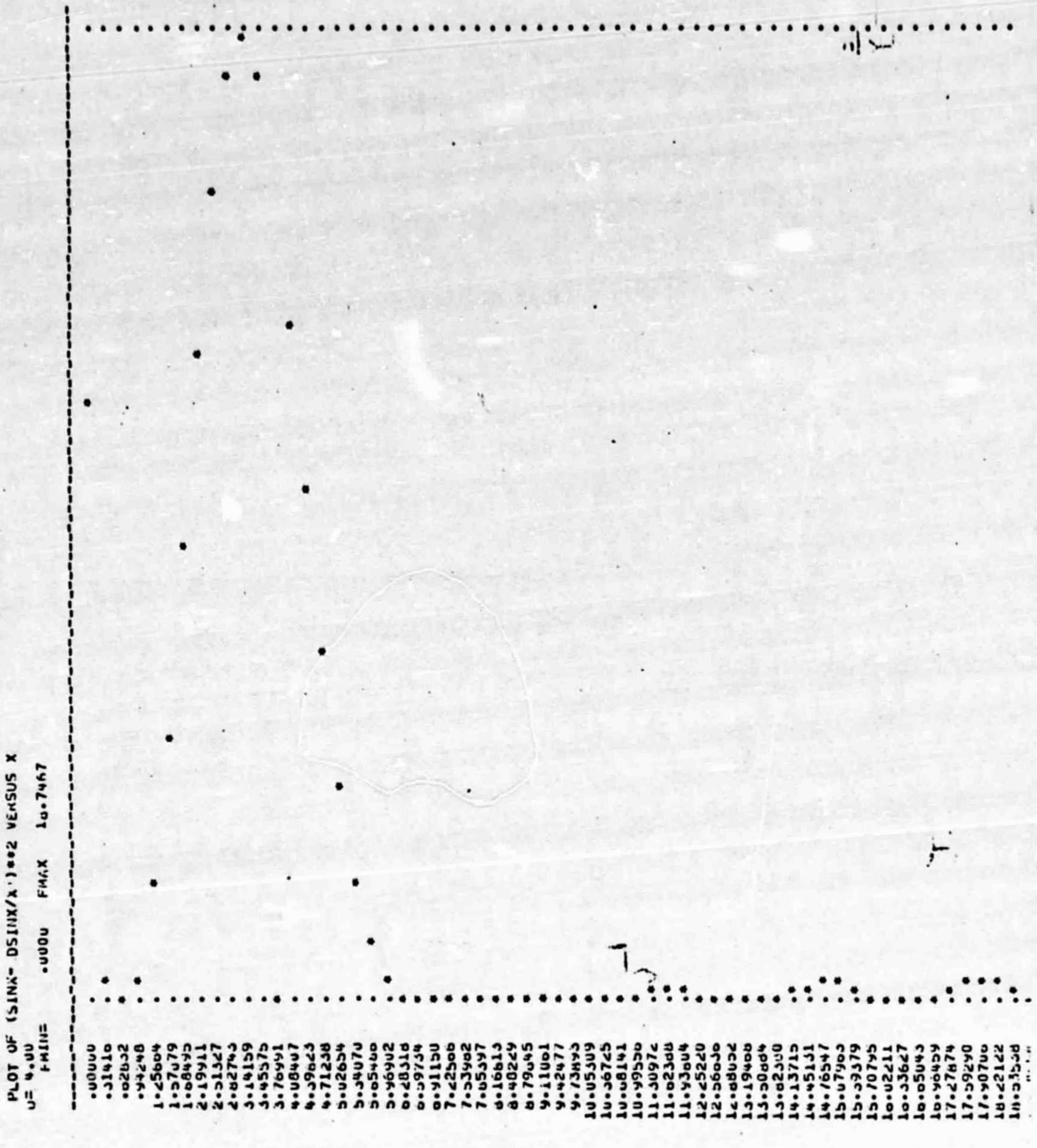

Figure 27

IV. Discussion

From the examples given in the last section, it can be seen that the examples in Sec.III indicate that the phase-modulated triple-exposure holographic interferometric technique can be used in the identification of the zero-order fringe and the determination of the direction of the displacement. Although the phase variation during the loading process was assumed to be linear with respect to time, the result would not be qualitatively different if other time dependence was assumed.

The incorporation of this technique into a HNDT system can be made by applying a removable phase-shifter to the object beam. A block diagram showing the phase-modulated HNDT system is given in Fig. 28. The operational procedure is described below. During the first exposure, the phase shifter P is removed from the object beam. The phase shifter is replaced into the object beam during the second and third exposures. The amount of phase shift may be different. For example, the phase shift during the second exposure may be π and that during the third exposure may be $\pi/2$. It should be noted that the phase-shifter may also be inserted into the reference beam instead.

If a flat (or quasi-flat) object is under test, the analysis of data can be made by concentrating our attention on the higher order fringes and use the principle that the fringe pattern is of the following form[7]

$$A(x^2 + y^2) + Bx + Cy = (n - \tfrac{1}{2})\lambda \quad , \tag{24}$$

where λ is the wavelength of light; n is a positive integer greater than or equal to 1; A, B, and C are system dependent parameters. It may be concluded that due to the fact that the zero-order fringe is not counted, a more accurate assessment of surface displacement in the HNDT system can be achieved.

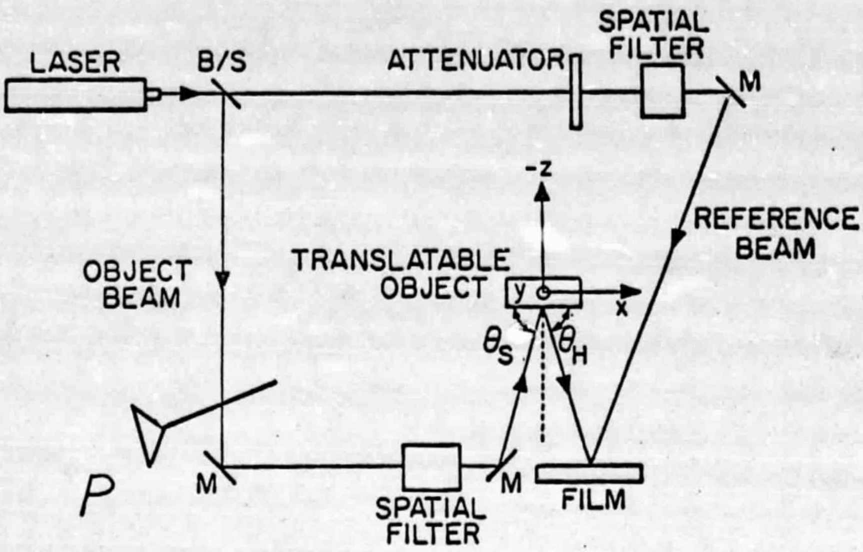

Figure 28. A block diagram for the phase-modulated HNDT system.

ORIGINAL PAGE IS
OF POOR QUALITY

APPENDIX A

Computer Programs

```
CPROGRAM 1
        DIMENSION P(1C2),F(100)
        INTEGER P,BLANK,STAR,DOT,DY,ZERO
        DATA BLANK,STAR,DOT/ ' ','*','.'/
        DATA ZERO/'0'/
          FMIN=999.9
        FMAX=-999.9
        DO 10 I=1,41
        DX=(I-1)*3.14159*0.1
        F(I)=(SIN(DX)/DX)**2
        IF(I.EQ.1) F(I)=1.0
        IF(F(I) .GT. FMAX) FMAX=F(I)
        IF (F(I) .LT. FMIN) FMIN=F(I)
10      CONTINUE
        P(1)= DOT
        P(102)=DOT
        DO 20 I=2,101
20      P(I)=BLANK
        WRITE(6,100) FMIN,FMAX
100     FORMAT( '1',1CX,'PLOT OF SINX**2/X**2 VERSUS X',/ ' ',5X,'SINX**2
       C/X**2',F8.2,95X,F8.2)
        SCALE=(FMAX-FMIN)*C.001
        MY=(-FMIN)/SCALE+1
        DY=50
        FI=FMIN+(50+MY)*SCALE
        FJ=FMIN+(MY-5C)*SCALE
        P(DY)=ZERO
        WRITE(6,104) FJ,(P(J),J=1,10C),FI
104      FORMAT(' ',16X,F5.3,100A1,F5.3)
        P(DY)=BLANK
        WRITE (6,101)
101     FORMAT ('0',1CX,115('-'))
        DO 30 I=1,81
        DX=(I-1)*3.14159*0.05
        DY=(F(I)-FMIN)/SCALE+1
        DY=DY-MY+50
        IF(DY.GT.101) GO TO 40
        IF(DY.LT.1) GC TO 40
        P(DY)=STAR
40      WRITE(6,102) DX,(P(J),J=1,102)
102     FORMAT ( ' ',5X,F12.5,4X,102A1)
        IF(DY.GT.101)GO TO 30
        IF (DY.EQ.1) P(DY)=DOT
        IF(DY.GT.1) P(DY)=BLANK
30      CONTINUE
        WRITE (6,101)
        WRITE(6,103)
103      FORMAT ('1')
         STOP
        END
```

```
      C PROGRAM 2
            DIMENSION P(102),F(80),A(3),D(4)
            INTEGER P,BLANK,STAR,DOT,DY,ZERO
            DATA BLANK,STAR,DOT/ ' ','*','.'/
            DATA ZERO/'0'/
            DATA (A(I),I=1,3)/ 0.5,0.8,1.0/
            DATA (D(I),I=1,4)/0.01,0.02,0.03,0.05/
              FMIN=999.9
            FMAX=-999.9
            DO 5 IA=1,3
            DO 7 IJ=1,4
            DO 10 I=1,61
            DX=(I-1)*3.14159*0.1
            DJ=D(IJ)*3.14159
            B=(A(IA)*SIN(DX+DJ)/(DX+DJ))**2
            F(I)=(SIN(DX)/DX)**2-B
            IF(I.EQ.1) F(I)=1-B
            IF(F(I) .GT. FMAX) FMAX=F(I)
            IF (F(I) .LT. FMIN) FMIN=F(I)
      10    CONTINUE
            P(1)= DOT
            P(102)=DOT
            DO 20 I=2,101
      20    P(I)=BLANK
            WRITE(6,100)
      100   FORMAT ('1',10X,'PLOT OF (SINX/X)**2-(A*SIN(X+D)/(X+D))**2 VERSUS
           CX')
            WRITE(6,99) A(IA),D(IJ),FMIN,FMAX
      99     FORMAT (' ',10X,'A=',F5.2,10X,'D=',F5.2,'PI',/' ',14X,'FMIN='
           C ,F10.4,3X,'FMAX=',F10.4)
            SCALE=(FMAX-FMIN)*0.001
            MY=(-FMIN)/SCALE+1
            DY=50
            FJ=FMIN+(MY-50)*SCALE
            FI=FMIN+(50+MY)*SCALE
            P(DY)=ZERO
            WRITE(6,104) FJ,(P(J),J=1,100),FI
      104    FORMAT(' ',16X,F5.3,100A1,F5.3)
            P(DY)=BLANK
            WRITE (6,101)
      101   FORMAT ('0',10X,115('-'))
            DO 30 I=1,41
            DX=(I-1)*3.14159*0.1
            DY=(F(I)-FMIN)/SCALE+1
            DY=DY-MY+50
            IF(DY.GT.101) GO TO 40
            IF(DY.LT.1) GO TO 40
            P(DY)=STAR
            P(DY)=STAR
      40    WRITE(6,102) DX,(P(J),J=1,102)
      102   FORMAT ( ' ',5X,F12.5,4X,102A1)
            IF(DY.GT.101)GO TO 30
            IF (DY.EQ.1) P(DY)=DOT
            IF(DY.GT.1) P(DY)=BLANK
      30    CONTINUE
            WRITE (6,101)
            WRITE(6,103)
      103    FORMAT ('1')
            FMAX=-999.9
              FMIN=999.9
      7     CONTINUE
      5     CONTINUE
             STOP
            END
```

ORIGINAL PAGE IS OF POOR QUALITY

PROGRAM No. 3

```
      CPROGRAM 3
            DIMENSION P(102),F(100)
            INTEGER P,BLANK,STAR,DOT,DY
            DATA BLANK,STAR,DOT/ ' ','*','.'/
              FMIN=999.9
            FMAX=-999.9
            DO 10 I=1,51
            DX=(I-1)*0.4
            BS=BSSL(DX,3)
            F(I)=(2*BS/DX)**2
            IF(F(I) .GT. FMAX) FMAX=F(I)
            IF (F(I) .LT. FMIN) FMIN=F(I)
   10       CONTINUE
            P(1)= DOT
            P(102)=DOT
            DO 20 I=2,101
   20       P(I)=BLANK
            WRITE(6,100) FMIN,FMAX
  100       FORMAT( '1',10X,'PLOT OF SINX**2/X**2 VERSUS X',/ ' ',5X,'SINX**2
           C/X**2',F8.2,95X,F8.2)
            WRITE (6,101)
  101       FORMAT ('0',10X,115('-'))
            SCALE=(FMAX-FMIN)*0.01
            DO 30 I=1,51
            DX=(I-1)*0.4
            DY=(F(I)-FMIN)/SCALE+1
            P(DY)=STAR
            WRITE(6,102) DX,(P(J),J=1,102)
  102       FORMAT ( ' ',5X,F12.5,4X,102A1)
            IF (DY.EQ.1) P(DY)=DOT
            IF(DY.GT.1) P(DY)=BLANK
   30       CONTINUE
            WRITE (6,101)
            WRITE(6,103)
  103        FORMAT ('1')
             STOP
            END
```

D. OF COMPILATION: NO DIAGNOSTICS.

ORIGINAL PAGE IS
OF POOR QUALITY

PROGRAM No. 4

```
      C PROGRAM 4
          DIMENSION P(102),F(60),A(3),D(4)
          INTEGER P,BLANK,STAR,DOT,DY
          DATA BLANK,STAR,DOT/ ' ','*','.'/
          DATA (A(I),I=1,3)/ 0.5,0.8,1.0/
          DATA (D(I),I=1,4)/0.1,0.4,0.8,2.0/
            FMIN=999.9
          FMAX=-999.9
          DO 5 IA=1,3
          DO 7 IJ=1,4
          DO 10 I=1,51
           DX=(I-1.0)*0.4
          BS=BSSL(DX,3)
          DJ=D(IJ)
          TX=DX+DJ
           BSD=BSSL(TX,3)
          B=(2*A(IA)*BS/TX)**2
          F(I)=(2*BS/DX)**2-B
          IF(F(I) .GT. FMAX) FMAX=F(I)
          IF (F(I) .LT. FMIN) FMIN=F(I)
   10     CONTINUE
          P(1)= DOT
          P(102)=DOT
          DO 20 I=2,101
   20     P(I)=BLANK
          WRITE(6,100)
  100     FORMAT ('1',10X,'PLOT OF (SINX/X)**2-(A*SIN(X+D)/(X+D))**2 VERSUS
         CX')
          WRITE(6,99) A(IA),D(IJ),FMIN,FMAX
   99      FORMAT (' ',10X,'A=',F5.2,10X,'J=',F5.2,'PI',/' ',14X,'FMIN='
         C ,F10.4,3X,'FMAX=',F10.4)
          WRITE (6,101)
  101     FORMAT ('0',10X,115('-'))
          SCALE=(FMAX-FMIN)*0.01
          DO 30 I=1,51
          DX=(I-1)*0.4
          DY=(F(I)-FMIN)/SCALE+1
          P(DY)=STAR
          WRITE(6,102) DX,(P(J),J=1,102)
  102     FORMAT ( ' ',5X,F12.5,4X,102A1)
          IF (DY.EQ.1) F(DY)=DOT
          IF(DY.GT.1) P(DY)=BLANK
   30     CONTINUE
          WRITE (6,101)
          WRITE(6,103)
  103      FORMAT ('1')
          FMAX=-999.9
            FMIN=999.9
    7     CONTINUE
    5     CONTINUE
           STOP
          END
```

OF COMPILATION: NO DIAGNOSTICS.

```
C PROGRAM 5
      DIMENSION P(102),F(130),D(4)
      INTEGER P,BLANK,STAR,DOT,DY
      DATA BLANK,STAR,DOT/ ' ','*','.'/
      DATA (D(I),I=1,4)/1.0,2.0,3.0,4.0/
        FMIN=999.9
      FMAX=-999.9
      DO 7 IJ=1,4
      DO 10 I=1,121
      DX=(I-1)*3.14159*0.1
      B=IJ**2*(SIN(DX))**2/(DX**2)
      F(I)=(SIN(DX))**2+B
      IF(I.EQ.1) F(I)=2.0
      IF(F(I) .GT. FMAX) FMAX=F(I)
      IF (F(I) .LT. FMIN) FMIN=F(I)
 10   CONTINUE
      SCALE=(FMAX-FMIN)*0.01
      P(1)= DOT
      P(102)=DOT
      DO 20 I=2,101
 20   P(I)=BLANK
      FMAX=100*SCALE
      WRITE(6,100)
 100  FORMAT ('1',10X,'PLOT OF (SINX)**2+D**2(SINX)**2/X**2 VERSUS X ')
      WRITE(6,99) D(IJ),FMIN,FMAX
 99   FORMAT (' ',10X,'D=',F5.2,'   ',/' ',14X,'FMIN=',F10.4,3X,'FMAX'
     C,F10.4)
      WRITE(6,101)
 101  FORMAT ('0',10X,115('-'))
       DO 30 I=1,121
      DX=(I-1)*3.14159*0.1
      DY=(F(I)-FMIN)/SCALE+1
      IF(DY.GT.101)GO TO 40
      P(DY)=STAR
 40   WRITE(6,102) DX,(P(J),J=1,102)
 102  FORMAT ( ' ',5X,F12.5,4X,102A1)
      IF (DY.EQ.1) P(DY)=DOT
      IF(DY.GT.101)GO TO 30
      IF(DY.GT.1) P(DY)=BLANK
 30   CONTINUE
      WRITE (6,101)
      WRITE(6,103)
 103   FORMAT ('1')
      FMAX=-999.9
        FMIN=999.9
 7    CONTINUE
      STOP
      END
```

ORIGINAL PAGE IS
OF POOR QUALITY

D OF COMPILATION: NO DIAGNOSTICS.

```
C PROGRAM 6
      DIMENSION P(102),F(250),D(4)
      INTEGER P,BLANK,STAR,DOT,DY
      DATA BLANK,STAR,DOT/ ' ','*','.'/
      DATA (D(I),I=1,4)/1.0,2.0,3.0,4.0/
       FMIN=999.9
      FMAX=-999.9
      DO 7 IJ=1,4
       DO 10 I=1,241
      DX=(I-13)*3.14159*0.1
      B=IJ*SIN(DX)/DX
      IF (I.EQ.1) B=IJ
      F(I)=(SIN(DX)-B)**2
      IF(F(I) .GT. FMAX) FMAX=F(I)
      IF (F(I) .LT. FMIN) FMIN=F(I)
   10 CONTINUE
      SCALE=(FMAX-FMIN)*0.01
      P(1)= DOT
      P(102)=DOT
      DO 20 I=2,101
   20 P(I)=BLANK
      FMAX=100*SCALE
      WRITE(6,100)
  100 FORMAT ('1',10X,' PLOT OF (SINX- DSINX/X )**2 VERSUS X ')
      WRITE(6,99) D(IJ),FMIN,FMAX
   99 FORMAT (' ',10X,'D=',F5.2,'  ',/' ',14X,'FMIN=',F10.4,3X,'FMAX'
     C,F10.4)

      WRITE(6,101)
  101 FORMAT ('0',10X,115('-'))
      DO 30 I=1,241
      DX=(I-1)*3.14159*0.1
      DY=(F(I)-FMIN)/SCALE+1
      IF(DY.GT.101)GO TO 40
      P(DY)=STAR
   40 WRITE(6,102) DX,(P(J),J=1,102)
  102 FORMAT ( ' ',5X,F12.5,4X,102A1)
      IF (DY.EQ.1) P(DY)=DOT
      IF(DY.GT.101)GO TO 30
      IF(DY.GT.1) P(DY)=BLANK
   30 CONTINUE
      WRITE (6,101)
      WRITE(6,103)
  103  FORMAT ('1')
      FMAX=-999.9
       FMIN=999.9
    7 CONTINUE
      STOP
      END

D OF COMPILATION:          NO  DIAGNOSTICS.
```

REFERENCES

1. Kurzzeitphotographie, Othmar Helwich, Ed., Druck: Roetherdruck, Darmstadt, 1967, pp. 440-442.

2. E. Hecht and A. Zazac, Optics, Addison-Wesley (May, 1975).

3. D. Gabor, G. W. Stroke, R. Restuck, A. Funkhouser, and D. Brumm, "Optical Image Synthesis (Complex Amplitude Addition and Subtraction) by Holographic Fourier Transformation", Phys. Lett., 18, 116 (1965).

4. U. Kopf, Opt. Laser Technol., 5, 111 (1973).

5. F. Gori and G. Guattari, Opt. Commun., 5, 359 (1972).

6. P. C. Gupta and A. K. Aggarwal, Appl. Opt., 15, 2961 (1976).

7. H. K. Liu and R. L. Kurtz, Opt. Engr., 16, 176-186 (1977).